Universidad de Valladolid

Escuela de Doctorado

CELLMAT

Trabajo Fin de Máster

Máster en Física

Effect of TPU chemistry and concentration on the cellular structure of nanocellular polymers based on PMMA/TPU blends

Autor:

Ismael Sánchez Calderón

Tutor/es:

Victoria Bernardo García y Miguel Ángel Rodríguez Pérez

Effect of TPU chemistry and concentration on the cellular structure of nanocellular polymers based on PMMA/TPU blends

Ismael Sánchez Calderón, Victoria Bernardo García, Miguel Ángel Rodríguez Pérez.

Cellular Materials Laboratory (CellMat), Condensed Matter Physics Department, University of Valladolid, Valladolid, Spain

RESUMEN

Los polímeros nanocelulares se caracterizan por tener tamaños de celda con tamaños de decenas o centenas de nanómetros y densidades celulares mayores de 10^{13} celdas/cm^3. Estos materiales han despertado gran interés en el área de la Ciencia de Materiales debido a sus interesantes propiedades, tales como su reducida conductividad térmica, sus mejores propiedades mecánicas y la posibilidad de producir materiales celulares con cierta transparencia. En este trabajo se han desarrollado polímeros nanocelulares basados en poli(metil-metacrilato) (PMMA) utilizando poliuretano termoplástico (TPU) como agente nucleante mediante espumado por disolución de gas. Se han empleado tres grados de TPU con diferente proporción de segmentos duros (60%, 70% y 80%) en diferentes contenidos (0.5%, 2% y 5% en peso con respecto al PMMA). En primer lugar, se ha estudiado la morfología de los materiales sólidos, observando que la fase de TPU se dispersa en la matriz de PMMA formando dominios nanométricos. Los materiales celulares en base PMMA/TPU se caracterizan por un gradiente de tamaños de celda, comenzando por una región microcelular en el borde de la muestra y reduciéndose el tamaño hasta alcanzar la parte central, que se caracteriza por estar compuesto de celdas nanométricas. La presencia de las celdas nanométricas se debe al efecto nucleante del TPU. Se ha caracterizado la estructura celular en estas muestras de PMMA/TPU. En concreto, se ha analizado cómo evolucionan los parámetros celulares en el core nanocelular (densidad relativa, tamaño de celda y densidad de nucleación) en función del contenido de TPU y de la proporción de segmentos duros en el TPU. Por un lado, al aumentar el contenido de TPU, la densidad de nucleación se incrementa, reduciéndose el tamaño de celda, debido al aumento del número de dominios de TPU en el sólido. Por otro lado, al aumentar la proporción de segmentos duros en el TPU, se observa la misma tendencia (la densidad de nucleación aumenta mientras que el tamaño de celda se reduce) y, en este caso, este resultado es debido a una mejor dispersión del TPU. Cuanto mayor contenido de segmentos duros, mayor es el peso molecular del TPU. A medida que el peso molecular del TPU se aproxima al del PMMA el tamaño de los dominios se reduce, aumentando la densidad de dominios. Se han obtenido polímeros nanocelulares con densidades relativas en la parte central de las muestras de entre 0.15 y 0.20 y tamaños de celda entre 220 y 640 nm.

ABSTRACT

Nanocellular polymers are characterized by cell sizes in the range of tens to hundreds of nanometers and cell densities greater than 10^{13} cells/cm^3. These materials have aroused great interest in the area of Materials Science due to their interesting properties, such as a reduced thermal conductivity, better mechanical properties and the possibility of producing cellular materials with a certain transparency. In this work, nanocellular polymers based on poly(methyl-methacrylate) (PMMA) have been produced by gas dissolution foaming using thermoplastic polyurethane (TPU) as a nucleating agent. Three grades of TPU with a different fraction of hard segments (60%, 70% and 80%) have been used in different contents (0.5 wt%, 2 wt% and 5 wt% in PMMA). First, the morphology of solid materials has been studied, observing that the TPU phase appears as a dispersed phase in the PMMA matrix forming nanometric domains. The PMMA/TPU foamed samples are characterised by a gradient of the cell size from the edge of the sample towards the core. The cells near the edges are micrometric and cells in the core are nanometric. The presence of the nanometric cells in the core is due to the nucleating effect of the TPU. The cellular structure has been characterised in these PMMA/TPU samples. Specifically, the evolution of the cellular parameters (relative density, cell size and cell nucleation density) have been analysed in the nanocellular core as a function of the TPU content and of the fraction of hard segments in the TPU. On the one hand, as the TPU content increases, the nucleation density increases, and the cell size is reduced due to the increment in the number of TPU domains dispersed in the solid. On the other hand, by increasing the fraction of hard segments in the TPU, the cell nucleation density increases, and the cell size is reduced due to a better dispersion of the TPU. As the content of hard segments increases, the molecular weight of the TPU is higher. In addition, as the molecular weight of the TPU approaches the PMMA molecular weight the size of the domains is reduced, increasing the density of domains. Nanocellular polymers have been obtained with a relative density between 0.15 and 0.20 and cell sizes between 220 and 640 nm.

Keywords: nanocellular polymer, poly(methyl-methacrylate); thermoplastic polyurethane; gas dissolution foaming.

1. Introduction

Cellular materials are two-phase structures in which a gas has been dispersed along a continuous solid phase so-called matrix[1]. The production of these materials allows expanding the range of applications of the solid that is used as a matrix. Within cellular materials, those that are manufactured from a polymeric matrix (cellular polymers) are of great technological interest, because they exhibit high impact energy absorption (they can be used for instance in packaging and body protection) and low thermal conductivities (they are used in the thermal insulation of buildings), among other properties[2,3]. These properties attached to their low weight and cost make

these materials to have a large presence in technological sectors such as construction, packaging, automotive, etc.

Nowadays, modern society needs specific materials for each application, so there is a need to develop new materials at the same pace as technology advances. The properties of cellular polymers depend on several factors, such as their density, morphology and cell size, properties of the solid matrix, etc. In this way, cellular polymers properties can be improved by modifying their cellular structure, and more specifically by reducing their cell size. This effect was shown first in the change of scale from conventional to microcellular polymers[2], and more recently in the development of nanocellular polymers.

Nanocellular polymers are characterised by cell sizes in the range of tens to hundreds of nanometers. As a consequence of their reduced cell size, these materials present a double confinement effect. On the one hand, the gas is confined in the nanometric pores, whereas the solid phase is constrained in very thin cell walls. As a result of these effects, nanocellular polymers have very interesting properties. For instance, when the cell size reaches values around the mean free path of the gas molecules contained in the pores (e.g. ~ 70 nm in case of air at room temperature and atmospheric pressure), the contribution of the conduction through the gas to the thermal conductivity of the material is drastically decreased due to the Knudsen effect[4]. The combination of this effect with a low-density would allow obtaining materials with very low thermal conductivities and significant applications in the thermal insulation industry[5,6]. Regarding the confinement of the solid phase, it can lead to significant changes in the behaviour of the material, such as an increase of the glass transition temperature or improvements in the mechanical properties[7,8]. Furthermore, nanocellular polymers produced from transparent polymers can keep, up to some extent, the transparent character of the former solid if the cell size is small enough (smaller than 50 nm), leading to the possibility of producing transparent thermal insulators[9]. Finally, due to their nanometric cell size, nanocellular materials with an interconnected cellular structure can also be employed in some specific applications in which conventional cellular materials cannot be used, like as membranes for micro and ultrafiltration or in catalysis and sensors[10,11]. For all these reasons, in recent years, nanocellular polymers have aroused great attention and are the new frontier for materials and polymer science.

The fabrication of nanocellular polymers is still a challenging task because it requires specific production routes able to produce and stabilize cells in the nanoscale. Among the diverse methods employed for this purpose[5,12,13] one of the most promising techniques is the so-called gas dissolution foaming[14]. In this method, a physical blowing agent, such as carbon dioxide (CO_2), is dissolved in the polymer and then, by a proper manipulation of the pressure and temperature, is used to produce thick nanocellular samples without using organic solvents or additional chemical

compounds. Therefore, from an industrial point of view, it seems to be the most promising approach to produce nanocellular polymers at large scales. The choice and design of the precursor polymer are crucial in the fabrication of nanocellular polymers by gas dissolution foaming. On the one hand, amorphous polymers with a high glass transition temperature are favourable due to their extremely large viscoelasticity, which can significantly restrict cell growth and prevent cell coalescence. On the other hand, polymers with a high CO_2 affinity are suitable to obtain high amounts of gas absorbed in the polymer matrix. In particular, CO_2 gas dissolution foaming has been proved to be adequate for the production of bulk nanocellular polymers using different matrices, such as poly(methyl-methacrylate) (PMMA)[9,15–17], polycarbonate (PC)[18], polyphenylsulfone (PPSU)[19,20], or polyetherimide (PEI)[21,22].

Particularly, to produce nanocellular polymers based on PMMA using the gas dissolution foaming method, two approaches can be followed according to the type of nucleation mechanism that takes place: homogeneous or heterogeneous nucleation. According to the homogeneous nucleation theories[23], the activation energy (Gibbs energy barrier) necessary to generate a nuclei can be decreased by maximizing the amount of CO_2 uptake in a pure polymer. However, this requires the use of highly demanding processing conditions such as high pressures or low saturation temperatures, that complicates the possible production of low-density nanocellular polymers on a large scale[9,15–17]. For instance, Martín-de León et al.[15] produced PMMA with a relative density of 0.24 and cell sizes around 200 nm using a high saturation pressure (31 MPa) and 25 ºC of saturation temperature. Guo et al.[17] achieved relative densities of 0.14 and average cell sizes of 235 nm employing a saturation pressure of 5 MPa and a low saturation temperature (-30 ºC) in a PMMA system. Otherwise, the nucleation can be enhanced by taking advantage of the heterogeneous nucleation mechanism. In this case, the use of an immiscible second phase allows decreasing the Gibbs energy barrier in the interfaces between the matrix and the second phase, promoting a higher nucleation ratio[23]. To produce nanocellular polymers with this approach, nanoparticles[24,25] or block copolymer micelles[10,26–28] can be used as the second phase. In this way, Costeux et al.[24] used silica nanoparticles to produce a low relative density (0.15) nanocellular PMMA (cell size of 100 nm), but the saturation pressure required was still high (30 MPa). Bernardo et al.[25] obtained bimodal micro and nanocellular structures at 10 MPa of saturation pressure and 25 ºC of saturation temperature, using a system based on PMMA and sepiolite nanoparticles. Materials with relative densities of 0.21-0.28 and cell sizes between 300 and 500 nm were obtained. On the other hand, Pinto et al.[10,26,27] worked with blends of PMMA and poly(methyl methacrylate)-poly(butyl acrylate)-poly(methyl methacrylate) (MAM) with MAM contents of 5 wt%, 10 wt% and 20 wt%. They showed that nucleation actually took place in the micelles[26] and that the cellular structure was controlled by the nanostructuration. In this case, the MAM micelles are CO_2-philic, so nucleation was also enhanced due to the action of the micelles

as CO_2 reservoirs. Cell sizes in the range 150–200 nm and relative densities of 0.4–0.6 were obtained in these works. In the same way, Forest et al.[28] studied PMMA/MAM blends observing a saturation effect on the nucleation (as the MAM content increases, the cell density increases until reaching a maximum value). They obtained nanocellular polymers with a cell size of 150 nm and relative densities around 0.42 using a MAM content of 1 wt% at 3.2 MPa of saturation pressure and 0 ºC of saturation temperature. Recently, Bernardo et al.[29] showed that these PMMA/MAM systems allow producing low-density nanocellular materials (cell size 350 nm, relative density 0.23) at 10 MPa of saturation pressure and 25 ºC of saturation temperature.

Another interesting system for the production of nanocellular polymers is the immiscible blend of PMMA with thermoplastic polyurethane (TPU) that results in a nanostructuration of the TPU phase. Wang et al.[30], obtained a nanocellular polymer based on a PMMA/TPU blend with a cell size of 205 nm and a relative density of 0.125, using a saturation pressure of 13.8 MPa and a saturation temperature of 25 ºC. In this paper, only one TPU grade was used and the homogeneity of the structure from the edge to the core of the samples was not studied in detail. However, they claimed that an additional cooling step before releasing the pressure was necessary to ensure a homogeneous cellular structure. Up to date, and despite the promising results reported in this work, this is the only work in the literature about the use of TPU as a nucleating agent in PMMA to produce nanocellular polymers.

On the other hand, the search for new structures with better properties, as happened with the evolution of the cell size from conventional to microcellular and then to nanocellular materials[14,31], has led scientists to try mimic natural structures. Nature structural porous materials (such as wood or bones) have a complex structure with a non-uniform cell density and/or morphology. In particular, cellular materials with a gradient cellular structure (i.e. a cellular structure that changes form the edge to the core of the sample) can confer superior properties and provide the basis for the development of new functions[32,33]. Several attempts to produce such structures have been developed recently. For instance, Pinto et al.[34] obtained cellular polymers with graded cell size taking advantage of the heterogeneous nucleation approach. To do this, they used templated solid PMMA samples with well-differentiated regions, presenting or not zinc oxide (ZnO) nanoparticles, by thermal in situ synthesis of ZnO nanoparticles from zinc acetate ($Zn(OAc)_2$). Nucleation was enhanced in the region with nanoparticles, causing a graded cellular structure. With the same aim, Trofa et al.[35] employed time-varying boundary conditions of the gas sorption stage to generate layered and graded cellular polymers based on polystyrene (PS). They show that, by designing the saturation step, it is possible to achieve non-trivial gas concentration profiles, so they obtained cellular polymers with controlled morphology profiles. Also, they produce a femur-like cellular polymer based on polycaprolactone (PCL), which is a biocompatible polyester extensively utilized in tissue engineering.

In this work, the effect of the TPU content and of the amount of hard segments (HS) in the TPU on the production of PMMA/TPU nanocellular polymers has been studied. TPU contents between 0.5 wt% and 5 wt% and three TPU grades with an amount of 60%, 70% and 80% of hard segments (HS) were investigated. Nanocellular polymers with a graded cellular structure and relative densities in the core of the samples between 0.15-0.20 and average cell sizes in the core of the samples ranging from 220 to 640 nm have been obtained.

2. Experimental

2.1. Materials

PMMA Plexiglas® 7N was kindly supplied by EVONIK in the form of pellets. This PMMA presents a melt flow index (*MFI*) of 3.58 g/10 min (measured at 230 °C and 2.16 kg), a density (ρ) of 1.19 g/cm^3, a glass transition temperature (T_g) of 108.4 ºC, measured by differential scanning calorimetry (DSC) (model DSC822e, Mettler) using a heating programme from 20 ºC to 160 ºC at a rate of 10 ºC/min, a number-average molecular weight (M_n) of 45000 g/mol and a weight-average molecular weight (M_w) of 84000 g/mol.

The TPU grades under study were synthesized at the Polymers & Peptides Research Group (University of Manchester, UK). Three TPU polymers with variable hard segments (HS) content were used in this study (60%, 70% and 80% of HS content). **Table 1** summarizes the main characteristics of these polymers. Density (ρ) was obtained by gas pycnometry (model AccuPyc II 1340, Micromeritics). Glass transition (T_g) of soft ($T_{g,SS}$) and hard segments ($T_{g,HS}$) and melting temperature (T_m) were determined by DSC with a heating programme from -90 ºC to 220 ºC at a heating rate of 10 ºC/min. Shore hardness D was measured by means of a Bareiss durometer model U/72, according to UNE-EN ISO 868[36]. Number-average molecular weight (M_n), weight-average molecular weight (M_w) and polydispersity index (M_w/M_n) were measured by gel permeation chromatography (GPC).

As seen in **Table 1**, TPU density, hardness, number-average molecular weight and weight-average molecular weight increases with the HS content. Also, the glass transition temperature of soft segments ($T_{g,SS}$) is only observed for the lowest content (60% of HS content), while $T_{g,HS}$ and T_m are almost equal for all the HS contents.

Finally, medical grade carbon dioxide (CO_2) (99.9% purity) was used as the blowing agent for the gas dissolution foaming experiments.

Table1. Characteristics of the TPU polymers used in this work.

Description	ρ (g/cm^3)	$T_{g,SS}$ (ºC)	$T_{g,HS}$ (ºC)	T_m (ºC)	Hardness (Shore D)	M_n (g/mol)	M_w (g/mol)	Polydispersity Index
60% HS	1.192	- 43.3	55.5	177.5	45.6 ± 0.5	8552 ± 1602	18325 ± 535	2.18 ± 0.32
70% HS	1.204	-	55.5	183.5	63.2 ± 0.4	14043 ± 1162	31449 ± 128	2.25 ± 0.20
80% HS	1.217	-	51.3	183.4	72.4 ± 0.5	15086 ± 2126	32603 ± 4825	2.16 ± 0.02

2.2. Solid blends production

PMMA/TPU blends with different TPU contents were compounded using a twin-screw extruder model COLLIN TEACH-LINE ZK 25T, with L/D of 24 and screw diameter of 25 mm. Before compounding, PMMA and TPU were dried in vacuum at 60 °C for 12 h. Then, the blends with the appropriate proportions were extruded with a temperature profile from 155 °C to 195 °C (in the die), increasing in intervals of 10 °C, and at a screw speed of 40 rpm. The produced blends were cooled in a water bath and pelletized. After drying the pellets, the materials were extruded again under the same conditions with the aim of homogeneously mixing the two components. In the second extrusion cycle, the extruded filament was set aside a let cool at room temperature. Blends with three different TPU contents, from 0.5 wt% to 5 wt%, of the three TPU grades were produced. **Table 2** summarizes the materials produced in this work. The cylindrical filament (that presents an average diameter of 3-4 mm) was cut in samples of 30 mm in length for the foaming experiments.

Neat PMMA was processed under the same conditions for the sake of comparison.

Table 2. Formulations used in this work and nomenclature.

		TPU content		
		0.5 wt%	2 wt%	5 wt%
Type of TPU	60% HS	0.5_60% HS	2_60% HS	5_60% HS
	70% HS	0.5_70% HS	2_70% HS	5_70% HS
	80% HS	0.5_80% HS	2_80% HS	5_80% HS

2.3. Gas dissolution foaming experiments

Foaming experiments were performed in a high-pressure vessel (model PARR 4681) provided by Parr Instruments Company with a capacity of 1 litre, capable of operating at a maximum temperature of 350 °C and a maximum pressure of 41 MPa. An accurate pressure pump controller (model SFT-10) provided by Supercritical Fluid Technologies Inc. controls automatically the

pressure to keep the desired value. The vessel is equipped with a clamp heater of 1200 W, and its temperature is controlled via a CAL 3300 temperature controller. With this set up foaming experiments were performed using a two-step gas dissolution foaming process[37]. This process consists of three steps: saturation, pressure release and foaming. Samples were firstly introduced in the pressure vessel under 15 MPa of CO_2 pressure and at 25 °C for the saturation stage. The saturation time was 20 h; this time is enough to ensure that the PMMA samples are fully saturated[26]. After saturation, the pressure was abruptly released using a pressure drop rate of 15 MPa/s during the first instants of the pressure drop. Then, samples were removed from the pressure vessel and immersed in a thermal bath at the desired foaming temperature for the foaming step. Foaming was carried out in a water bath at 90 °C for 1 min (see **Supplementary Information Section S1** for details about the selection of the foaming temperature). The time between the release of pressure and the immersion of samples in the baths was 2 min.

Note that, under these saturation conditions (25 °C and 15 MPa), the effective glass transition temperature of PMMA after the gas absorption is below room temperature[26], so samples start to expand immediately after the release of pressure. Nevertheless, this expansion is clearly smaller than that taking place when the samples are introduced in the thermal bath at 90ºC.

2.4. Characterization

2.4.2. Nanostructuration

The nanostructuration of the solid samples was analysed using a Scanning Electron Microscope (FlexSEM 1000 VP-SEM). With the aim of maintaining the structure for the microscopic visualization, samples were cooled in liquid nitrogen and fractured. Afterwards, a chemical etching was performed using tetrahydrofuran (THF) for 30 minutes. THF dissolves faster the TPU phase than the PMMA, revealing the nanostructuration. Finally, the samples were coated with gold using a sputter coater (model SCD 005, Balzers Union). A tool based on the software ImageJ/FIJI[38] was used to quantify the structural parameters. TPU domain density (N_d) was determined according to equation (1), where A is the analysed area and n_d is the number of domains in that area. In every region, more than 150 domains were analysed. Also, the average domain size (ϕ_d) was obtained by measuring the diameter of the domains.

$$N_d = \left(\frac{n_d}{A}\right)^{3/2} \quad (1)$$

2.4.1. Density

The density of the solid samples was measured with a gas pycnometer (model AccuPyc II 1340, Micromeritics). The density of the corresponding cellular materials was determined with the water-displacement method based on Archimedes' principle. A density determination kit for an

AT261 Mettler-Toledo balance has been used for this purpose. Relative density (ρ_r) was calculated as the ratio between the cellular material density (ρ_f) and the density of the corresponding solid polymer (ρ_s). Some of the samples of this work present a graded cellular structure as shown schematically in **Fig. 1**, that shows that there is solid skin in the surface of the samples (approximately 5 µm in thickens), a transition region where cells are microcellular and a core region in which the cells are nanocellular. The thickness of the transition region, named as "gradient distance" (equation (2)), is the distance between the edge of the sample (r_{sample}) and the homogeneous nanocellular core (r_{core}). Then, to account for this heterogeneity, the density of the foamed samples was determined twice. Firstly, the density of the complete foamed sample (as removed from the thermal bath and after waiting enough time to assure that the remaining gas had diffused out) was determined, and using this density a global relative density was measured ($\rho_{r,g}$). Secondly, the transition region (red region in **Fig. 1**) was removed with a polisher (model LaboPOl2-LaboForce3, Struers), the density was measured again and with this new value, the relative density of the homogeneous core (blue region in **Fig. 1**) was determined ($\rho_{r,c}$). The thickness of the transition region to be removed was determined with SEM image analysis. Also, for the PMMA, which no present a clear gradient cellular structure, we removed sample thickness until reaching a radius of 0.75 mm. This distance is into the core of all PMMA/TPU samples being a good reference for the measure of the core density.

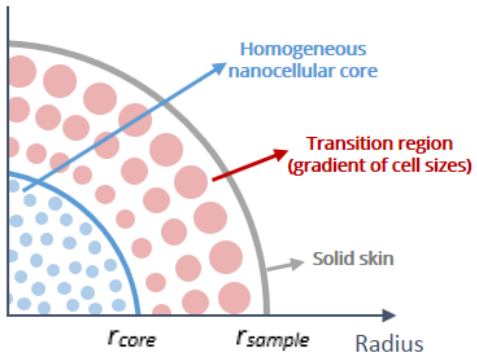

Fig. 1. Schematic structure of the cylindrical samples obtained in this work.

$$\text{Gradient Distance} = r_{sample} - r_{core} \quad (2)$$

2.4.2. Cellular structure

The cellular structure of the samples was analysed using a Scanning Electron Microscope (FlexSEM 1000 VP-SEM). With the aim of maintaining the cellular structure for the microscopic visualization, samples were cooled in liquid nitrogen and fractured. They were also coated with gold using a sputter coater (model SCD 005, Balzers Union). Several parameters were measured

in order to obtain a complete analysis of the cellular structure. Due to the gradient structure of the samples (as shown in **Fig. 1**), SEM images were taken at different distances along the sample radius (in a transversal direction to the extrusion direction) and the structure was analysed along the sample radius, and particularly in the nanocellular core. A tool based on the software ImageJ/FIJI[38] was used to quantify the structural parameters. Firstly, the average cell size in 3D (ϕ_{3D}), the cell size distribution and the standard deviation coefficient of the cell size distribution (SD) were obtained (3D values were obtained by multiplying the 2D values measured in the image by the correction factor 1.273[38]). The parameter SD/ϕ (normalised standard deviation coefficient) was calculated as an indicator of the homogeneity of the cellular structure. This parameter is used for comparison between materials with different cell size. Cell density (N_v) was determined using Kumar's theoretical approximation[39] according to equation (3), where *A* is the analysed area and *n* is the number of cells in that area. In every region, more than 200 cells were analysed.

$$N_v = \left(\frac{n}{A}\right)^{3/2} \tag{3}$$

In the core of the sample, that presents homogeneous cells, the cell nucleation density (N_0) was determined using equation (4) using the relative density of the core ($\rho_{r,c}$). This relation assumes that there are not degeneration effects of the structure during the foaming (that is, that every nucleation point in the solid becomes a cell in the foamed material).

$$N_0 = \frac{N_v}{\rho_{r,c}} \tag{4}$$

Also, some of the samples presented a bimodal structure with micrometric pores among the nanocellular structure. To characterize these samples, the fraction of area occupied by the micrometric cells in the SEM images has been measured. The criterion to classify a cell as micrometric was that: a cell is micrometric when is larger than five times the average value of cell size of the nanocellular region of that material.

3. Results and discussion

3.1. Nanostructuration of the blends

Fig. 2 shows a photograph of the solid samples produced in this work. As seen in **Fig. 2** by increasing the TPU content, the samples become more opaque. Also, for a fixed TPU content, the samples become more opaque by increasing the fraction of HS in the TPU. This effect is due to the dispersion of the TPU in the PMMA matrix. Furthermore, the transparency of the samples is an indicator of a well dispersion of the TPU phase.

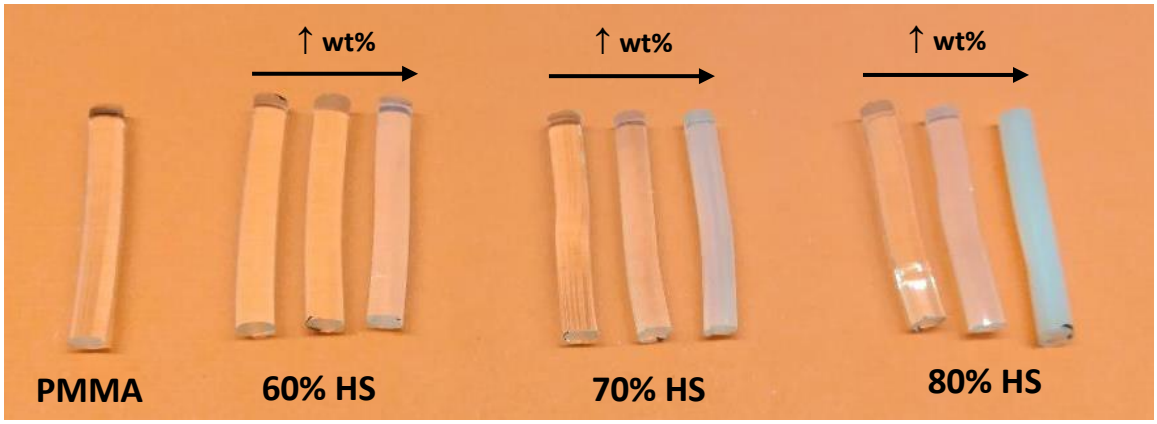

Fig. 2. Photograph of the solid samples produced in this work.

Fig. 3 shows representative SEM images of the chemical etched materials taken at the centre of the solid samples. We observe that at low TPU contents (0.5 wt% and 2 wt%) the etching does not reveal the TPU phase. However, at 5 wt% of TPU, the etching clearly shows the nanostructuration (the holes correspond to the TPU phase that is dissolved during the etching). **Table 3** summarizes the nanostructuration characteristics of these samples with 5 wt% of TPU (average domain size and domain density). As seen in the images, TPU form nanometric spherical domains. It is observed that increasing the HS content on the TPU increases the domain density, while the domain size is reduced. This effect is due to the molecular weight of the TPU. Higher molecular weights are associated with higher viscosities, and according to the model proposed by Wu[40], when a polymer of viscosity η_d is dispersed in a matrix of viscosity η_m (with $\eta_m > \eta_d$ because the PMMA presents higher molecular weight than the TPU (see **Section 2.1**)), the dispersed phase will form domains of size d determined by equation (5), where σ is the interphase surface tension and $\dot{\gamma}$ the shear velocity of the extruder screws. So, according to this equation, for a fixed polymer matrix and extrusion conditions, the size of the domains will decrease by increasing the viscosity (molecular weight) of the dispersed polymer. For a fixed amount of dispersed phase, a smaller domain size implies a higher domain density. This theoretical behaviour matches with the results of **Table 3**, and it was also observed in other systems[41]. The difference in TPU domain size between the blends with the TPU with an amount of HS of 60% and the one with an 70% of HS (160 nm versus 104 nm) is greater than the difference between the TPU grades with 70% and 80% of HS (104 nm versus 95 nm). The reason is that these two TPU grades present more similar molecular weights (**Table 1**).

$$d = \frac{\sigma \cdot 4}{\eta_m^{0.16} \cdot \dot{\gamma} \cdot \eta_d^{0.84}} \quad (5)$$

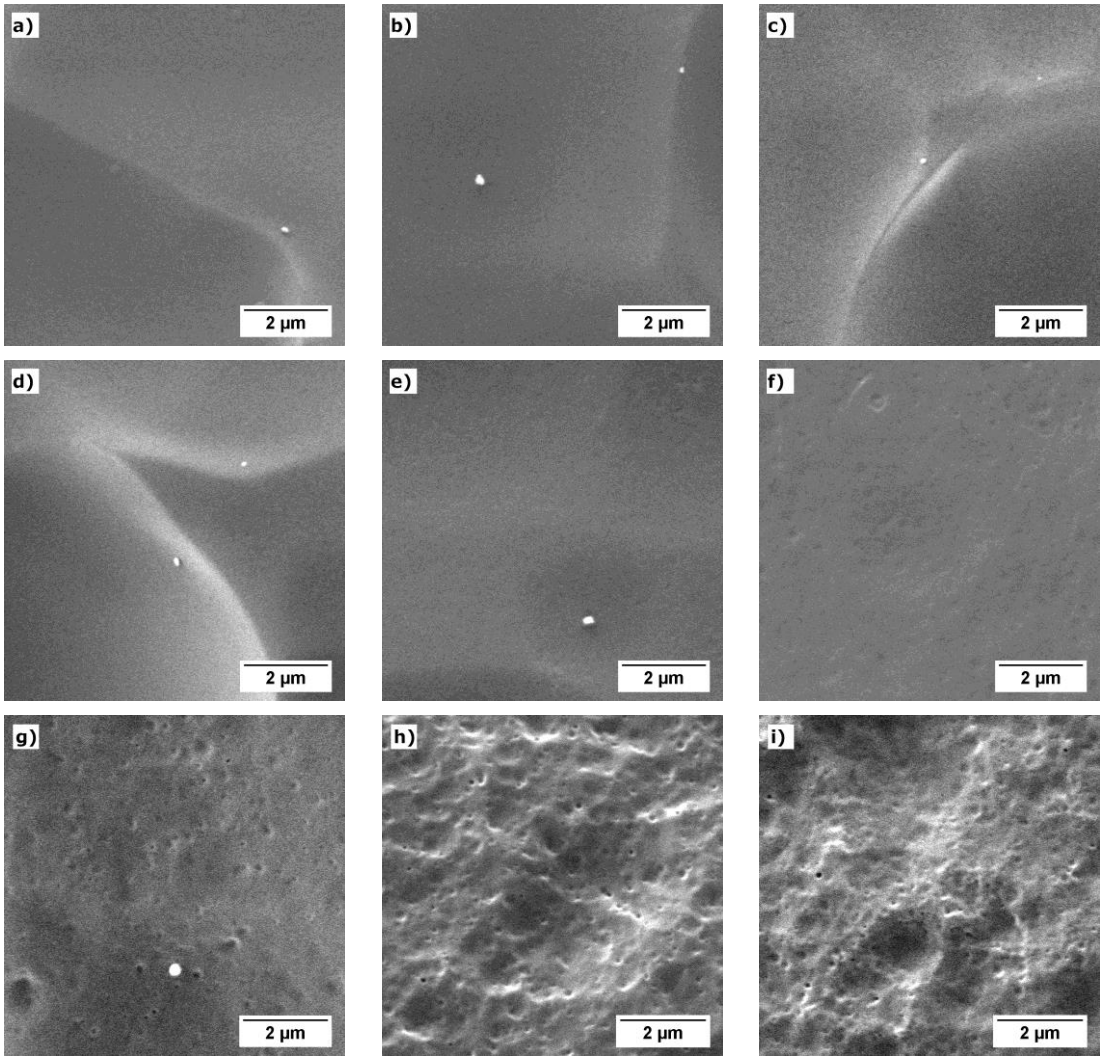

Fig. 3. Representative SEM images of the chemical etched materials taken at the centre of the solid sample: a) 0.5_60% HS, b) 0.5_70% HS, c) 0.5_80% HS, d) 2_60% HS, e) 2_70% HS, f) 2_80% HS, g) 5_60% HS, h) 5_70% HS and i) 5_80% HS.

Table 3. Nanostructuration characteristics of the thee PMMA/TPU solid samples with 5wt% of TPU produced in this work.

Material	ϕ_d (nm)	SD/ϕ_d	N_d (nulcei/cm^3)
5_60% HS	160	0.33	$2.3 \cdot 10^{13}$
5_70% HS	104	0.19	$4.0 \cdot 10^{13}$
5_80% HS	95	0.15	$1.2 \cdot 10^{14}$

3.2. Morphology of the foamed samples and effect of the addition of TPU

Fig. 4 shows representative SEM images taken at increasing distances from the edge to the centre of the samples of the cellular materials based on the blend 2_70% HS (**Fig. 4a**) and of the pure PMMA sample (**Fig. 4b**). The radial distance (r_d), defined as the ratio between the distance from the centre of the sample to the point of observation divided by the simple radius, has been taken

for the sake of comparison because samples had different radius. As shown in **Fig. 5**, where the evolution of the cell density (**Fig. 5a**) and of the cell size (**Fig. 5b**) is presented, the cellular material 2_70% HS presents a gradient cellular structure. The material is microcellular near the edge and becomes nanocellular in the core. All the PMMA/TPU samples produced in this work shows such a graded structure (except the material 5_80% HS which has a particular cellular structure explained in the **Supplementary Information Section S2** related to its nanostructuration but also present a gradient and a well-defined core). Furthermore, it is observed that the cellular structure of the PMMA sample is almost constant along the sample radius and is clearly heterogeneous and microcellular. Moreover, comparing **Fig. 4a.4** and **Fig. 4b.4**, that correspond to the core region of each sample, it is observed that the addition of TPU has a nucleating effect in PMMA. Thus, in the sample which contains TPU the cell density increases o values about 10^{13} cells/cm^3 (**Fig. 5a**) at the time the cell size is reduced to the nanometric scale (around 350 nm) when the core of the sample is reached (**Fig. 5b**).

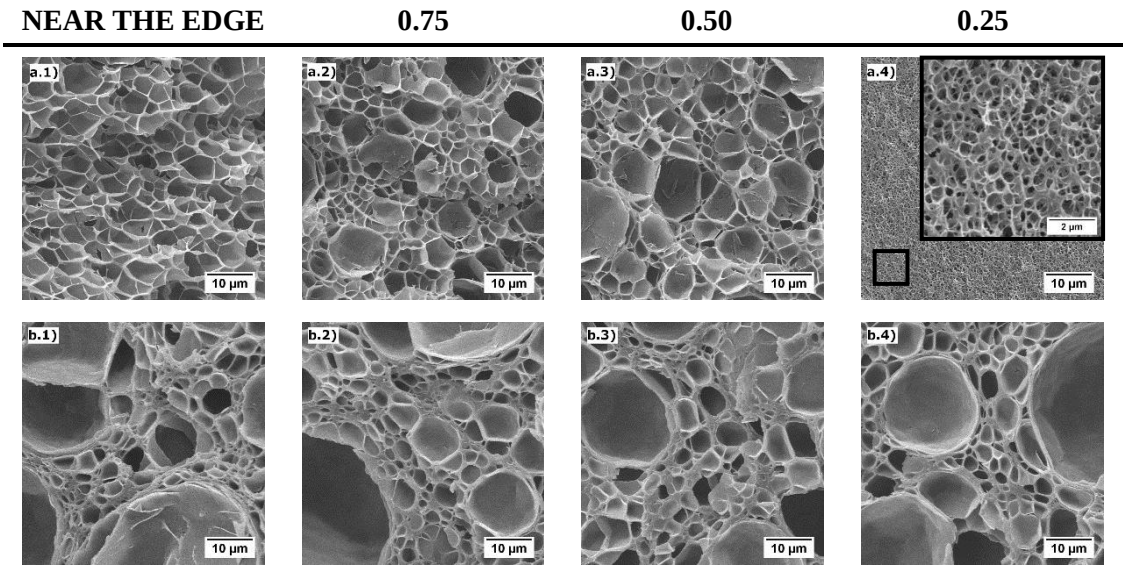

Fig. 4. Representative SEM images of the cellular materials: a) 2_70% HS and b) pure PMMA sample, in a transversal direction to the extrusion direction. Each image is taken at increasing distance from the edge to the centre of the sample along the sample radius (a.1 and b.1 NEAR THE EDGE (r_d ~ 1); a.2 and b.2: r_d ~ 0.75; a.3 and b.3: r_d ~ 0.50; a.4 and b.4: r_d ~ 0.25). Images a.4 and b.4 have been taken in the core of the samples.

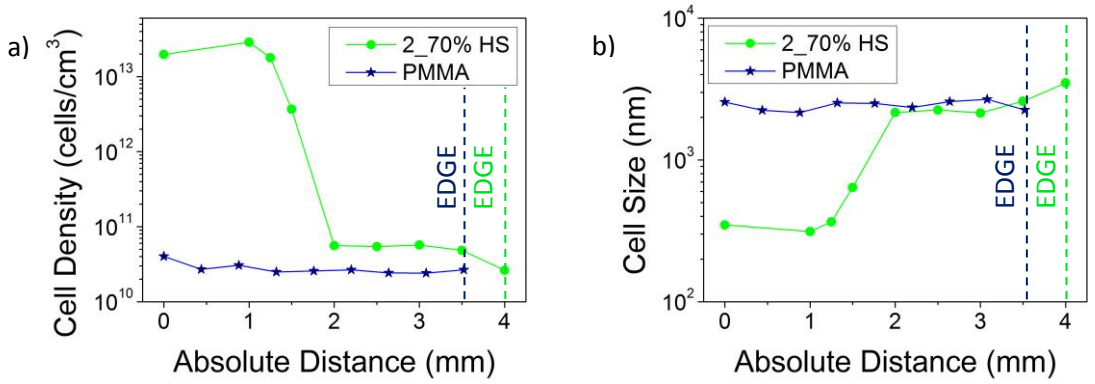

Fig. 5. a) Cell density and b) cell size of the cellular samples as a function of the radial distance from the centre (0 mm) to the edge of the 2_70% HS and PMMA.

The appearance of this gradient structures in the PMMA/TPU samples may be due to various causes. On the one hand, it could be caused by a heterogeneous dispersion of the TPU phase in the solid material. However, the gradient structure also appears in the longitudinal (extrusion) direction (see **Supplementary Information Section S3** for details about the gradient structure in the longitudinal direction). So, the TPU dispersion is not the reason under the appearance of the gradient structure. Another possible reason, that also explains the appearance of the gradient structure in the longitudinal direction, is the CO_2 diffusion outwards the sample during the desorption time (time between the pressure release and the foaming) (see **Section 2.3**). In this way, after the pressure release the sample starts to lose gas through the surface, so a gradient of gas concentration (or pressure gradient) appears from the edge towards the centre of the sample. Creating a non-constant gas concentration profile is a known strategy to produce gradient cellular structures[35]. This hypothesis was tested and verified by performing experiments with pre-cooling of the autoclave before the pressure released to delay the diffusion process (see details of this additional experiment in **Supplementary Information Section S4.1**). Also, it can explain the morphology of the PMMA because this material shows similar cellular structures when it is produced at 5 and 15 MPa[42].

A gas concentration profile (pressure gradient) seems to explain these samples morphology. In the centre of the samples, where the pressure is constant, the TPU act as a nucleating agent and increases the nucleation density. However, as pressure is reduced, nucleation in the TPU phase seems not to be predominant anymore. Then, we can conclude that the efficiency of the nucleation in the TPU phase reduces with decreasing pressure, leading to graded cellular structures. This is in agreement with nucleation theories. The nucleation process involves a critical radius (r_c)[26,43]: a nuclei with a radius larger than the critical radius would grow, otherwise, it tends to disappear. It is defined according to equation (6), where γ is the surface tension of the system and Δp is the pressure difference between the gas phase and the polymeric phase. In this way, as the pressure

difference increases the critical radio decreases (equation (6)), so the nucleation efficiency depends on pressure. Furthermore, the ratio between the radius of the nucleating species (*R*) and the critical radius plays a key role in the reduction of the energy barrier in a heterogeneous nucleation process[44,45]. So, as pressure increases, from the edge to the centre, the two radii get closer and the efficiency of the nucleation in the TPU phase increases. The fact that the values of the cell density and of the cell size of the cellular material 2_70% HS approach to the values of the PMMA sample outside the core reinforce this idea (**Fig. 5**).

$$r_c = \frac{2\gamma}{\Delta p} \tag{6}$$

3.3. Effect of the concentration of TPU and of the fraction of HS

Table 4 summarizes the global and core relative densities of the foamed samples produced with the different PMMA/TPU blends of **Table 2** and the pure PMMA. Also, **Table 4** includes the gradient distance (equation (2)) and the volume fraction that the nanocellular core fills in the total foamed sample. The fact that all the samples present an almost constant gradient distance (between 2-3 mm) reinforces the hypothesis of a pressure gradient as responsible for the appearance of this graded structure. The gradient cell size leads to a difference between the global density ($\rho_{r,g}$) and the core density ($\rho_{r,c}$). The core relative density is around 50% higher than the global relative density. Furthermore, **Fig. 6** shows the global and core relative density of the foamed samples (**Fig. 6a**) and the average global and core relative density as a function of the TPU grade (**Fig. 6b**). It is observed that PMMA global relative density does not coincide with the core relative density. So, this sample also shows a gradient structure, even though this is not so evident in the cell size and cell density measurement, because otherwise, the global and core relative densities should be similar. Further experiments and analysis are needed to understand this result.

Focusing on the core relative density of these PMMA/TPU materials, the pure polymer presents the highest relative density (**Table 4**). So, the addition of TPU reduces the relative density. The trend with the amount of TPU differs among the three TPU polymers. First, for the TPU with the lowest amount of HS (60% HS) increasing the TPU content reduces the core relative density from 0.206 for 0.5 wt% content to 0.174 for a 5 wt% content (**Table 4**). Meanwhile, the core relative density of the TPU with 70% of HS reaches a minimum of 0.156 for a 2 wt% content of TPU (**Table 4**). Finally, for the TPU with the highest amount of HS (80%), increasing the TPU content increases the core relative density from 0.153 for 0.5 wt% content to 0.202 for a 5 wt% content (**Table 4**). Also, taking the average relative density as a function of the TPU grade (**Fig. 6b**) it is observed that the relative densities are reduced when the HS of the TPU is increased reaching a minimum value for the materials with 70% of hard segments. On the other hand, an increase in the amount of TPU seems to increase the volume fraction of the core region.

Table 4. Relative density (global and core), gradient distance and core volume fraction of the foamed samples.

Sample ID	$\rho_{r,g}$	$\rho_{r,c}$	Gradient Distance (mm)	Volume Fraction (%)
PMMA	0.147 ± 0.001	0.225 ± 0.002	-	-
0.5_60% HS	0.143 ± 0.000	0.206 ± 0.002	3.0	5
2_60% HS	0.138 ± 0.001	0.200 ± 0.001	3.0	7
5_60% HS	0.148 ± 0.000	0.174 ± 0.002	2.0	22
0.5_70% HS	0.123 ± 0.001	0.177 ± 0.001	2.5	14
2_70% HS	0.107 ± 0.000	0.156 ± 0.005	2.7	10
5_70% HS	0.139 ± 0.001	0.171 ± 0.002	2.0	27
0.5_80% HS	0.110 ± 0.001	0.153 ± 0.001	3.0	8
2_80% HS	0.134 ± 0.000	0.191 ± 0.000	2.6	15
5_80% HS	0.152 ± 0.000	0.202 ± 0.001	2.5	15

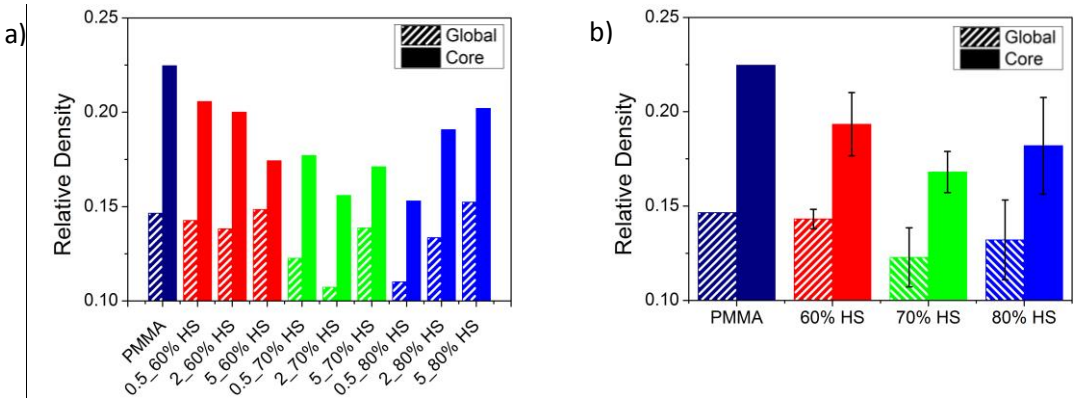

Fig. 6. a) Global and core relative density of the foamed samples and b) average global and core relative density as a function of the TPU grade.

Fig. 7 shows the SEM images of the core region of PMMA/TPU samples. Also, **Table 5** summarizes the data obtained after the cellular structure characterization, such as cell size (ϕ), cell nucleation density (N_0) of the nanocellular region and fraction of bimodality (fraction of area occupied by micrometric cells in this nanocellular region). Most of the PMMA/TPU samples show a nanocellular core (recall that all of them presented a graded structure as presented in the example of **Fig. 4a**). Only the material 0.5_60% HS shows cells larger than 700 nm with a wide cell size distribution (SD/ϕ_{3D} of 1.08), while for the rest of materials the parameter SD/ϕ_{3D} takes values between 0.45 and 0.65, which informs us of materials with an acceptable homogeneity of the nanocellular structure (**Table 5)**. Also, some of the samples present a bimodal structure, even though, for the highest content of TPU (5 wt%) all the samples are monomodal and nanocellular

(see **Supplementary Information Section S5** for details about the cell size distributions). For example, for the TPU with a 60% HS content the fraction of area of micrometric cells increases from 28% to 33% when the TPU content increases from 0.5 wt% to 2 wt%, but the cell size of the microcells is reduced more than four times (from 18.2 μm to 4.4 μm) (**Table 5**). The TPU which contains a 70% of HS only present bimodality at 0.5 wt% content (cells of 5 μm filling an area of 30%), being monomodal at the other contents (2 wt% and 5 wt%). Finally, for the blends based on the TPU with 80% of HS, the cell size of the microcells is reduced from 4.9 μm to 3.5 μm and the area fraction decreases from 14% to 3% when TPU content increases from 0.5 wt% to 2 wt% (**Table 5**).

Several reasons might explain the bimodality. First, it may be due to a heterogeneous dispersion of the TPU phase, but this has not been observed in the solid samples. On the other hand, the samples suffer a prefoaming before the foaming step (i.e. they start growing before they are heated up in the thermal batch (see **Section 2.3**)). Some of the cells might start growing during the desorption step (the larger ones) and the rest (the nanometric cells) during the foaming. So, not all the cells grow at the same time in the water bath causing a double population. To investigate this, a test with a cooling step before the pressure release has been carried out to reduce the prefoaming (see **Supplementary Information Section S4.2** for details about this experiment and its effect on the bimodality). After this experiment, in which we proved that the bimodality is reduced by preventing prefoaming, we conclude that prefoaming is one of the main causes of the bimodality.

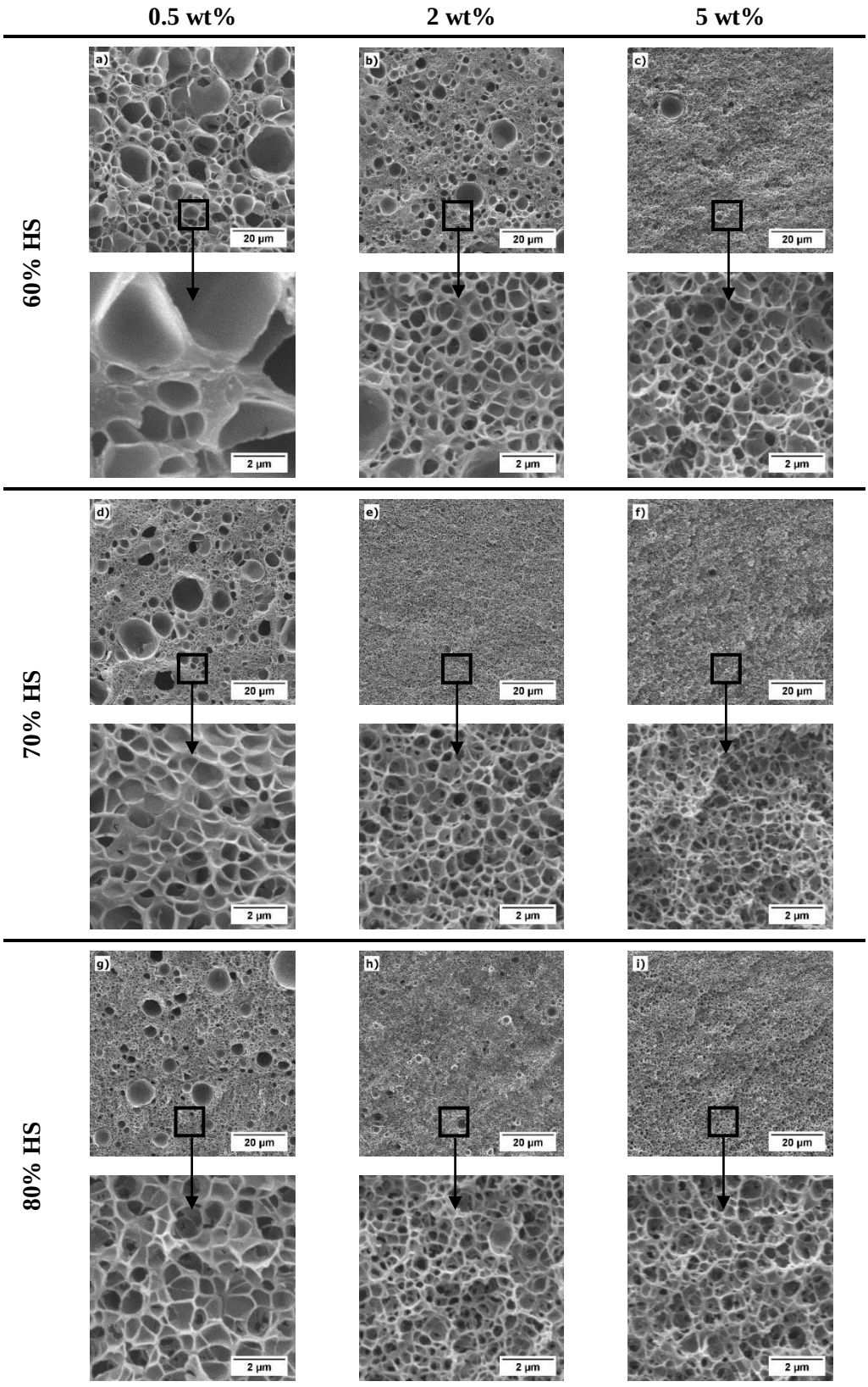

Fig. 7. SEM images of the core of the PMMA/TPU samples: a) 0.5_60% HS, b) 2_60% HS, c) 5_60% HS, d) 0.5_70% HS, e) 2_70% HS, f) 5_70% HS, g) 0.5_80% HS, h) 2_80% HS and i) 5_80% HS. The second row of each series correspond to high magnification images.

Table 5. Cellular structure characteristics of the core of the foamed samples.

				Bimodality		
Sample ID	N_0 (nulcei/cm^3)	ϕ_{3D} (nm)	SD/ϕ_{3D}	Area (%)	ϕ (µm)	SD/ϕ
0.5_60% HS	$(8.5 \pm 1.9) \cdot 10^{11}$	1417	1.08	28	18.2	0.40
2_60% HS	$(6.0 \pm 0.8) \cdot 10^{13}$	414	0.47	33	4.4	0.75
5_60% HS	$(8.7 \pm 0.5) \cdot 10^{13}$	359	0.64	-	-	-
0.5_70% HS	$(2.3 \pm 0.9) \cdot 10^{13}$	638	0.52	30	4.9	0.63
2_70% HS	$(1.3 \pm 0.0) \cdot 10^{14}$	348	0.52	-	-	-
5_70% HS	$(4.1 \pm 0.1) \cdot 10^{14}$	217	0.57	-	-	-
0.5_80% HS	$(3.2 \pm 0.3) \cdot 10^{13}$	591	0.48	14	4.9	0.50
2_80% HS	$(1.7 \pm 0.0) \cdot 10^{14}$	292	0.49	3	3.5	0.37
5_80% HS	$(7.2 \pm 2.2) \cdot 10^{13}$	373	0.62	-	-	-

Regarding the analysis of the nanocellular region, in **Fig. 8** the evolution of the cell nucleation density (**Fig. 8a**) and the cell size (**Fig. 8b**) is plotted as a function of the TPU content. For the TPU with 60% of HS, the cell nucleation density increases 70 times between the contents of 0.5 wt% and 2 wt%, reaching $8.7 \cdot 10^{13}$ nuclei/cm^3 at 5 wt% content (**Table 5**). On the other hand, cell size is reduced from 1417 nm to 359 nm when TPU content increases from 0.5 wt% to 5 wt%. The TPU with an amount of HS of 70% presents the same trends, by increasing the TPU content the cell nucleation density increases, and the cell size is reduced. At a concentration of 5 wt%, this TPU (70% of HS) reaches a cell nucleation density of $4.1 \cdot 10^{14}$ nuclei/cm^3 and a cell size of 217 nm (**Table 5**). Finally, the blends with TPU with 80% of HS follow the same trend for TPU contents between 0.5 wt% and 2 wt%, achieving the highest cell nucleation density and the lowest cell size at 2 wt% ($1.7 \cdot 10^{14}$ nuclei/cm^3 and 292 nm respectively). All the previous trends can be explained with the TPU domain density: increasing TPU content increases the TPU domain density, which causes higher nucleation and thus a smaller cell size. However, at 5 wt% of TPU, the nucleation density decreases to $7.2 \cdot 10^{13}$ nuclei/cm^3 and the cell size increases to 373 nm. This may be due to different reasons: on the one hand, an excessive number of generated nuclei that lead to structural degeneration mechanisms such as coalescence; and on the other hand, an excess of TPU content that produces agglomeration of the TPU dispersed phase during the extrusion or during the saturation step. The cellular structure does not seem degenerated (**Fig. 9**), so coalescence is discarded. In the cellular material 5_80% HS the TPU aggregates can be observed clearly (**Fig. 9**), while in other samples they cannot be seen. Then, the domains are bigger than in other blends (domain size around 150 nm). However, in a previous section, it has been seen that in the centre of the corresponding solid sample the nanometric domains were smaller (around 90 nm, **Table 5**). So, our hypothesis for this particular system is that the TPU agglomerates during the saturation step. During the saturation, the polymer is in a rubber state and an excessive number

of domains close to each other may permit them to agglomerate. As a result, the effective nucleation in this system is reduced. Further experiments are needed to prove this hypothesis.

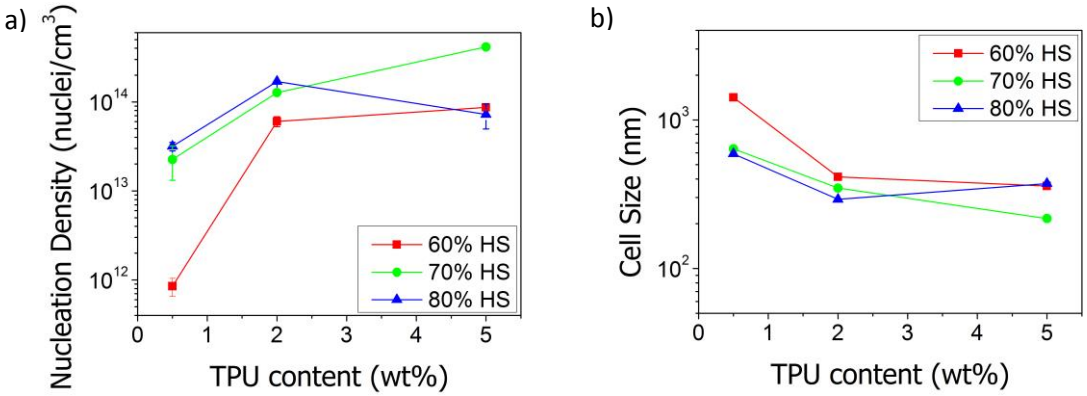

Fig. 8. a) Cell nucleation density and b) cell size as a function of the TPU content.

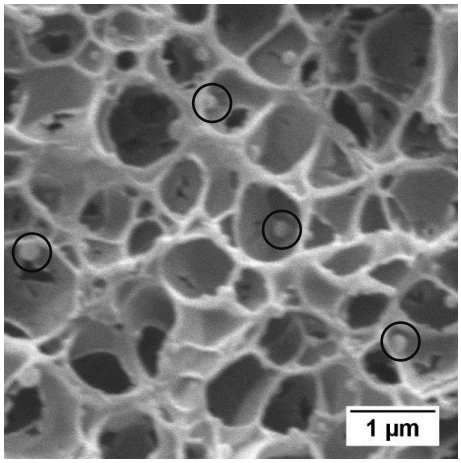

Fig. 9. TPU nanostructuration (5_80% HS).

From another point of view, the evolution of the cell nucleation density (**Fig. 10a**) and cell size (**Fig. 10b**) is represented in **Fig. 10** as a function of the amount of HS in the TPU. For the content of 0.5 wt%, increasing the amount of HS on the TPU increases de cell nucleation density and reduces the cell size. Specifically, between the contents of 60% and 70% of HS, there is a difference of more than 20 times in the cell nucleation density ($8.5 \cdot 10^{11}$ nuclei/cm^3 versus $2.3 \cdot 10^{13}$ nuclei/cm^3) and the cell size is reduced to half, from 1417 nm to 638 nm (**Table 5**). At 80% of HS content, a cell nucleation density of $3.2 \cdot 10^{13}$ nuclei/cm^3 and an average cell size of 591 nm are reached. For a TPU content of 2 wt%, the trend is the same, achieving a cell nucleation density of $1.7 \cdot 10^{14}$ nuclei/cm^3 and an average cell size of 292 nm for the TPU which contains an 80% HS. By last, for the content of 5 wt% the cell nucleation density increases (from $8.7 \cdot 10^{13}$ nuclei/cm^3 to $4.1 \cdot 10^{14}$ nuclei/cm^3) and the cell size decrease (from 359 nm to 217 nm) when the amount of HS increases from 60% to 70%. However, between the contents of 70% HS and 80% HS the cell nucleation density is reduced and the cell size increases, achieving $7.2 \cdot 10^{13}$ nuclei/cm^3 and 373

nm (**Table 5**). As already mentioned, this may be due to the agglomeration of TPU domains during the saturation step. Therefore, the amount fraction of HS in the TPU (that determines the molecular weight and the viscosity of the polymer) also plays an important role in the cellular structure. The cell sizes of the materials based on the TPU with lower HS content (lower viscosity) are larger than the rest and presenting smaller cell nucleation densities, as is already proved in other systems[41]. Furthermore, as commented previously, there is a higher difference between the TPUs with 60% and 70% of HS than between the 70% and the 80% HS because of the molecular weights of 70% and 80 % HS are closer in value.

Summarising, higher TPU contents and higher amount of HS in the TPU lead to higher density of TPU domains in the PMMA/TPU blend, which results in higher cell nucleation densities and smaller cell sizes. Also, the bimodality is reduced when TPU domain density increases. As the number of domains increases the distance among them is reduced and therefore there is less space for the cells to grow (resulting in lower cell sizes). It is also interesting to point out that the reduction of cell sizes reached by increasing the hard segment content are accompanied by density reduction (see **Fig. 6**).

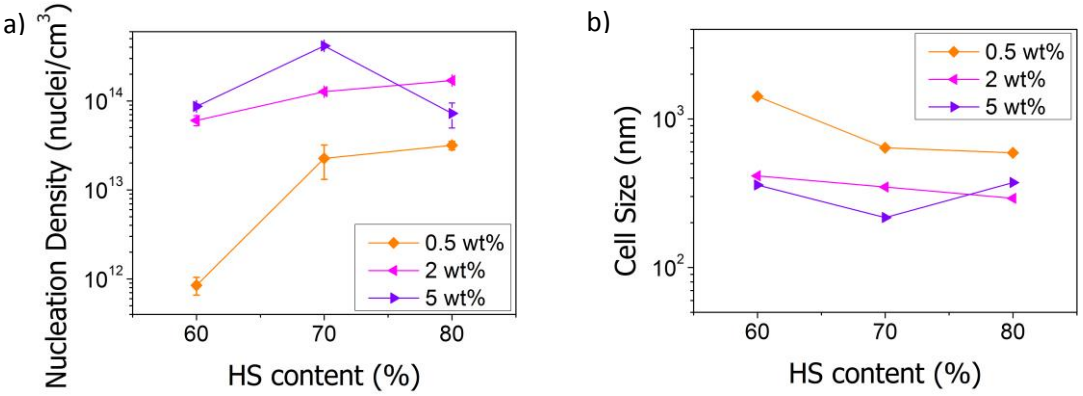

Fig. 10. a) Cell nucleation density and b) cell size as a function of the HS content.

Finally, **Fig. 11** shows the cell sizes of the nanocellular region as a function of the global and core relative density (**Fig. 11a** and **Fig. 11b** respectively) for all the samples produced in this work, classified according to the different amounts of HS in the TPU phase. According to this plot, the samples with the lowest relative density combined with the lowest cell size are the materials 0.5_80% HS (0.110 of global relative density, 0.153 of core relative density and average cell size of 591 nm) and 2_70% HS (0.107 of global relative density, 0.156 of core relative density and average cell size of 348 nm) (**Tables 4 and 5**). However, recall that the material 0.5_80% HS showed a bimodal cellular structure (**Table 5**).

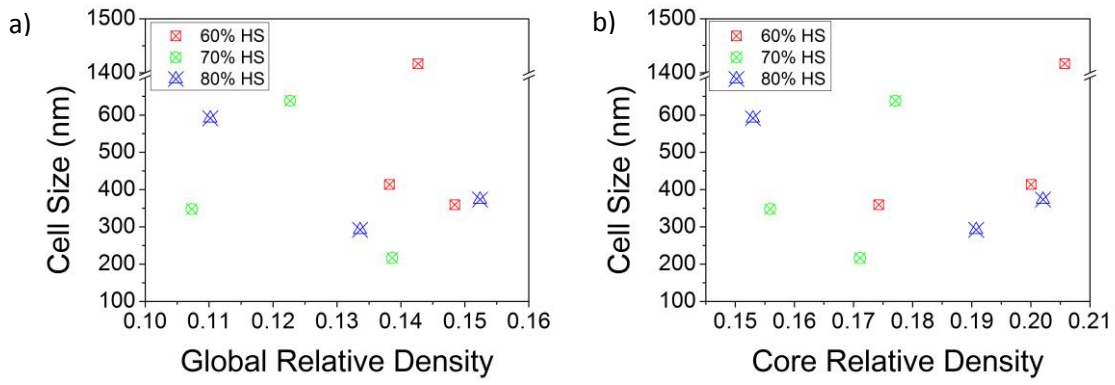

Fig. 11. Cell size in the nanocellular region – relative density map for all the samples produced in this work for the different TPU grades: a) global relative density and b) core relative density.

4. Conclusions

Low-density nanocellular polymers based on PMMA/TPU blends have been produced by means of a gas dissolution foaming process. Three grades of TPU with different amount of HS (60%, 70% and 80 %) were used. Blends with TPU contents of 0.5 wt%, 2 wt% and 5 wt% were produced by extrusion. As a result of the dispersion of the TPU in the PMMA matrix (immiscible blend), the solid material presents a nanostructuration formed by nanometric TPU domains. For a fixed TPU content, as the viscosity (molecular weight) of the TPU get closer to the PMMA viscosity the dispersion is favoured (the domain density increases and the domain size is reduced).

The morphology of the PMMA/TPU cellular materials is characterised by a gradient cell size distribution from the edge of the sample towards the core, from micrometric cells to nanocellular structures. While for the PMMA sample the cellular structure is almost constant along the sample radius being heterogeneous and microcellular. Moreover, in the core region, it is observed that the addition of TPU has a nucleating effect in PMMA. Thus, in the core of the samples which contains TPU the cell density increases at the time the cell size is reduced to the nanometric scale. On the other hand, it has been proved that the gradient cellular structure is caused by the diffusion of the gas out of the sample during the time gap between the release of the pressure and the beginning of foaming, that generates a gas concentration gradient (pressure gradient). Thus, in the centre of the samples, where the pressure is constant and high, the TPU act as a nucleating agent and increases the nucleation density. However, as pressure is reduced, nucleation in the TPU phase seems not to be predominant anymore.

In the analysis of the effect of the TPU content and of the fraction of HS on the cellular structure, a reduction of the relative density was detected with respect to the pure PMMA in the PMMA/TPU samples. Fist, the core cellular structure of some samples presents a double population of cells that is caused by the prefoaming. Thus, some of the cells might start growing

during the desorption step (the larger ones) and the rest (the nanometric cells) during the foaming. So, not all the cells grow at the same time in the water bath causing the bimodality. On the one hand, results show that by increasing the concentration of TPU, the cell nucleation density increases, and the cell size is reduced due to the increment of the number of domains of TPU dispersed in the solid. For example, for the TPU with a 60% of HS, the cell nucleation density increases 70 times between the contents of 0.5 wt% and 2 wt% while the cell size is reduced from 1417 nm to 414 nm. On the other hand, as the amount of HS in the TPU increase, the cell nucleation density increases and the cell size, as a result of the increase of the molecular weight (that favour the dispersion). For this reason, the TPUs with 70% and 80% of HS present close cell nucleation density and cell size at, for example, 2 wt% ($1.3 \cdot 10^{14}$ nuclei/cm^3 and $1.7 \cdot 10^{14}$ nuclei/cm^3 for the TPU with 70% and 80% of HS respectively) than the TPU with 60% HS ($6.0 \cdot 10^{13}$ nuclei/cm^3) because of their molecular weights are closer in value. However, an excess of TPU domains may cause an agglomeration during the saturation, reducing the cell nucleation density as seen for the material 5_80% HS where the cell nucleation density decreases from $1.7 \cdot 10^{14}$ nuclei/cm^3 at 2 wt% to $7.2 \cdot 10^{13}$ nuclei/cm^3 at 5 wt%. Also, the bimodality is reduced when TPU domain density increases because distance among them is reduced and therefore there is less space for the cells to grow (resulting in lower cell sizes).

Finally, a promising homogeneous material with nanocellular core with a relative density of 0.156 and a cell size of 348 nm was obtained.

Acknowledgements

I would like to thank Prof. Dr. Miguel Ángel Rodríguez Pérez for giving me the opportunity to do this work.

Thanks to Victoria Bernardo for her daily help, support and advice, and for teaching me with kind patience.

Finally, I would like to thank all my colleagues at CellMat Laboratory for their work, help and affection. Especially to Mercedes Santiago for lending me the TPUs that she synthesised.

Appendix A. Supplementary information

Supplementary information related to this article can be found after the references.

References

1. Gibson LJ, Ashby MF. Cellular Solids: Structure and Properties. *Cambridge Univ Press Cambridge*. 1997.

2. Eaves D. Handbook of Polymer Foams. *Rapra Tech*. 2004.

3. Saiz-Arroyo C, J.A. de Saja, Rodríguez-Pérez MA. Production and Characterization of Crosslinked Low-Density Polyethylene Foams using Waste of Foams with the Same Composition. *Polym Eng Sci*. 2012;52:751-759. doi:10.1002/pen

4. Li Z-Y, Zhu C-Y, Key X-PZ. A theoretical and numerical study on the gas-contributed thermal conductivity in aerogel. *Int J Heat Mass Transf*. 2017;108:1982-1990. doi:10.1016/j.ijheatmasstransfer.2017.01.077

5. Notario B, Pinto J, Rodriguez-Perez MA. Nanoporous polymeric materials: A new class of materials with enhanced properties. *Prog Mater Sci*. 2016;78-79:93-139. doi:10.1016/j.pmatsci.2016.02.002

6. Notario B, Pinto J, Solorzano E, de Saja JA, Dumon M, Rodríguez-Pérez MA. Experimental validation of the Knudsen effect in nanocellular polymeric foams. *Polymer (Guildf)*. 2015;56:57-67. doi:10.1016/j.polymer.2014.10.006

7. Pinto J, Notario B, Verdejo R, Dumon M, Costeux S, Rodriguez-Perez MA. Molecular confinement of solid and gaseous phases of self-standing bulk nanoporous polymers inducing enhanced and unexpected physical properties. *Polym (United Kingdom)*. 2017;113:27-33. doi:10.1016/j.polymer.2017.02.046

8. Notario B, Pinto J, Rodríguez-Pérez MA. Towards a new generation of polymeric foams: PMMA nanocellular foams with enhanced physical properties. *Polym (United Kingdom)*. 2015;63:116-126. doi:10.1016/j.polymer.2015.03.003

9. Martín-de León J, Bernardo V, Rodríguez-Pérez MÁ. Key Production Parameters to Obtain Transparent Nanocellular PMMA. *Macromol Mater Eng*. 2017. doi:10.1002/mame.201700343

10. Pinto J, Dumon M, Rodriguez-Perez MA, Garcia R, Dietz C. Block copolymers self-assembly allows obtaining tunable micro or nanoporous membranes or depth filters based on PMMA; Fabrication method and nanostructures. *J Phys Chem C*. 2014;118(9):4656-4663. doi:10.1021/jp409803u

11. Lu GQ, Zhao XS. NANOPOROUS MATERIALS - AN OVERVIEW. In: *Nanoporous Materials: Science and Engineering*. Imperial College Press; 2004.

12. Hentze H, Antonietti M. Porous polymers and resins for biotechnological and biomedical applications. *Handb porous solids*. 2002;90:27-53.

13. Hillmyer MA. Nanoporous materials from block copolymer precursors. *Adv Polym Sci*. 2005;190(1):137-181. doi:10.1007/12_002

14. Costeux S. CO2-blown nanocellular foams. *J Appl Polym Sci*. 2014;131:41293(1)-41293(27). doi:10.1002/app.41293

15. Martín-de León J, Bernardo V, Rodríguez-Pérez M ángel. Low density nanocellular polymers based on PMMA produced by gas dissolution foaming: Fabrication and cellular structure characterization. *Polymers (Basel)*. 2016;8(7). doi:10.3390/polym8070265

16. Guo H, Kumar V. Solid-state poly(methyl methacrylate) (PMMA) nanofoams. Part I: Low-temperature CO2 sorption, diffusion, and the depression in PMMA glass transition. *Polym (United Kingdom)*. 2015;57:157-163. doi:10.1016/j.polymer.2014.12.029

17. Guo H, Nicolae A, Kumar V. Solid-state poly(methyl methacrylate) (PMMA) nanofoams. Part II: Low-temperature solid-state process space using CO2 and the resulting morphologies. *Polym (United Kingdom)*. 2015;70:231-241. doi:10.1016/j.polymer.2015.06.031

18. Guo H, Kumar V. Some thermodynamic and kinetic low-temperature properties of the PC-CO2 system and morphological characteristics of solid-state PC nanofoams produced with liquid CO2. *Polym (United Kingdom)*. 2015;56:46-56. doi:10.1016/j.polymer.2014.09.061

19. Bernardo V, Martín-De León J, Rodríguez-Pérez MA. Production and characterization of nanocellular polyphenylsulfone foams. *Mater Lett*. 2016;178:155-158. doi:10.1016/j.matlet.2016.05.002

20. Guo H, Nicolae A, Kumar V. Fabrication of high temperature polyphenylsulfone nanofoams using high pressure liquid carbon dioxide. *Cell Polym*. 2016;35(3):119-142. doi:10.1177/026248931603500302

21. Miller D, Chatchaisucha P, Kumar V. Microcellular and nanocellular solid-state polyetherimide (PEI) foams using sub-critical carbon dioxide I. Processing and structure. *Polymer (Guildf)*. 2009;50:5576–5584. doi:10.1016/j.polymer.2011.04.049

22. Miller D, Kumar V. Microcellular and nanocellular solid-state polyetherimide (PEI) foams using sub-critical carbon dioxide II. Tensile and impact properties. *Polymer (Guildf)*. 2011;52(13):2910-2919. doi:10.1016/j.polymer.2011.04.049

23. Kalikmanov VI. Nucleation Theory. *Springer*. 2013.

24. Costeux S, Zhu L. Low density thermoplastic nanofoams nucleated by nanoparticles. *Polym (United Kingdom)*. 2013;54(11):2785-2795. doi:10.1016/j.polymer.2013.03.052

25. Bernardo V, Martín-de León J, Laguna-Gutiérrez E, Rodríguez-Pérez MÁ. PMMA-

sepiolite nanocomposites as new promising materials for the production of nanocellular polymers. *Eur Polym J*. 2017;96(June):10-26. doi:10.1016/j.eurpolymj.2017.09.002

26. Pinto J, Dumon M, Pedros M, Reglero J, Rodriguez-Perez MA. Nanocellular CO2 foaming of PMMA assisted by block copolymer nanostructuration. *Chem Eng J*. 2014;243:428-435. doi:10.1016/j.cej.2014.01.021

27. Pinto J, Reglero-Ruiz JA, Dumon M, Rodriguez-Perez MA. Temperature influence and CO2 transport in foaming processes of poly(methyl methacrylate)-block copolymer nanocellular and microcellular foams. *J Supercrit Fluids*. 2014;94:198-205. doi:10.1016/j.supflu.2014.07.021

28. Forest C, Chaumont P, Cassagnau P, Swoboda B, Sonntag P. CO2 nano-foaming of nanostructured PMMA. *Polym (United Kingdom)*. 2015;58:76-87. doi:10.1016/j.polymer.2014.12.048

29. Bernardo V, Martin-de Leon J, Pinto J, Catelani T, Athanassiou A, Rodriguez-Perez MA. Low-density PMMA / MAM nanocellular polymers using low MAM contents : Production and characterization. *Polymer (Guildf)*. 2019;163(August 2018):115-124. doi:10.1016/j.polymer.2018.12.057

30. Wang G, Zhao J, Mark LH, et al. Ultra-tough and super thermal-insulation nanocellular PMMA/TPU. *Chem Eng J*. 2017;325(May):632-646. doi:10.1016/j.cej.2017.05.116

31. Janani H, M.H.N. Famili. Investigation of a Strategy for Well Controlled Inducement of Microcellular and Nanocellular Morphologies in Polymers. *Polym Eng Sci*. 2010;50:1158-1570. doi:10.1002/pen

32. Ghaffari Mosanenzadeh S, Naguib HE, Park CB, Atalla N. Design and development of novel bio-based functionally graded foams for enhanced acoustic capabilities. *J Mater Sci*. 2015;50(3):1248-1256. doi:10.1007/s10853-014-8681-6

33. Monnereau L, Urbanczyk L, Thomassin JM, et al. Gradient foaming of polycarbonate/carbon nanotube based nanocomposites with supercritical carbon dioxide and their EMI shielding performances. *Polymer (Guildf)*. 2015;59:117-123. doi:10.1016/j.polymer.2014.11.063

34. Pinto J, Morselli D, Bernardo V, et al. Nanoporous PMMA foams with templated pore size obtained by localized in situ synthesis of nanoparticles and CO2 foaming. *Polymer (Guildf)*. 2017;124:176-185. doi:10.1016/j.polymer.2017.07.067

35. Trofa M, Di Maio E, Maffettone PL. Multi-graded foams upon time-dependent exposition to blowing agent. *Chem Eng J*. 2019;362(October 2018):812-817.

doi:10.1016/j.cej.2019.01.077

36. 868 U-EI. Determinación de la dureza de indentación por medio de un durómetro (dureza Shore). Plásticos y ebonita. AENOR; 2003. p. 11.

37. Kumar V, Suh NP. A process for making microcellular thermoplastic parts. *Polym Eng Sci*. 1990;30(20):1323-1329. doi:10.1002/pen.760302010

38. Pinto J, Solórzano E, Rodriguez-Perez MA, De Saja JA. Characterization of the cellular structure based on user-interactive image analysis procedures. *J Cell Plast*. 2013;49(6):555-575. doi:10.1177/0021955X13503847

39. Kumar V. Process synthesis for manufacturing microcellular thermoplastic parts. *Massachusetts Inst Technol*. 1988.

40. Wu S. Formation of dispersed phase in incompatible polymer blends: Interfacial and rheological effects. *Polym Eng Sci*. 1987;27(5):335-343. doi:10.1002/pen.760270506

41. Bernardo V, Martin-de Leon J, Laguna-Gutierrez E, et al. Understanding the role of MAM molecular weight in the production of PMMA / MAM nanocellular polymers. *Polymer (Guildf)*. 2018;153(August):262-270. doi:10.1016/j.polymer.2018.08.022

42. Sánchez-Calderón I. Desarrollo de polímeros nanocelulares basados en PMMA utilizando TPU como agente nucleante. *Trab Fin Grado*. 2018;(Julio).

43. Khan I, Adrian D, Costeux S. A model to predict the cell density and cell size distribution in nano-cellular foams. *Chem Eng Sci*. 2015;138:634-645. doi:10.1016/j.ces.2015.08.029

44. Fletcher NH. Size Effect in Heterogeneous Nucleation. *J Chem Phys*. 1958;29. doi:10.1063/1.1744540

45. Zhai W, Yu J, Wu L, Ma W, He J. Heterogeneous nucleation uniformizing cell size distribution in microcellular nanocomposites foams. *Polymer (Guildf)*. 2006;47(21):7580-7589. doi:10.1016/j.polymer.2006.08.034

Supplementary Information

Effect of TPU chemistry and concentration on the cellular structure of nanocellular polymers based on PMMA/TPU blends

Ismael Sánchez Calderón, Victoria Bernardo García, Miguel Ángel Rodríguez Pérez.

Cellular Materials Laboratory (CellMat), Condensed Matter Physics Department, University of Valladolid, Valladolid, Spain

S1. Preliminary study: selection of the foaming temperature

A preliminary study was carried out to select the foaming temperature. A gas dissolution foaming experiment under the same saturation parameters used for the samples in the paper (15 MPa and 25 ºC) was conducted. In this test, the foaming temperature was selected between three temperatures (80 ºC, 90 ºC and 100 ºC). The samples used in this experiment were the pure PMMA and the PMMA/TPU blend with a 70% amount of HS in 2 wt% content (2_70%HS).

Fig. S1 shows the evolution of the global and core relative densities (**Fig. S1a** and **Fig. S1b** respectively) of the cellular materials produced as a function of the foaming temperature. At 80 ºC and 90 ºC, the PMMA/TPU samples present lower global and core relative densities than the PMMA. At 100 ºC the PMMA present the lowest core relative density (0.15), but the sample split in half. Furthermore, between 90 ºC and 100 ºC no significant differences are observed in the core relative densities for the TPU sample (around 0.16). So, a foaming temperature of 90 ºC was selected as the optimum to avoid possible degeneration mechanisms at higher temperatures.

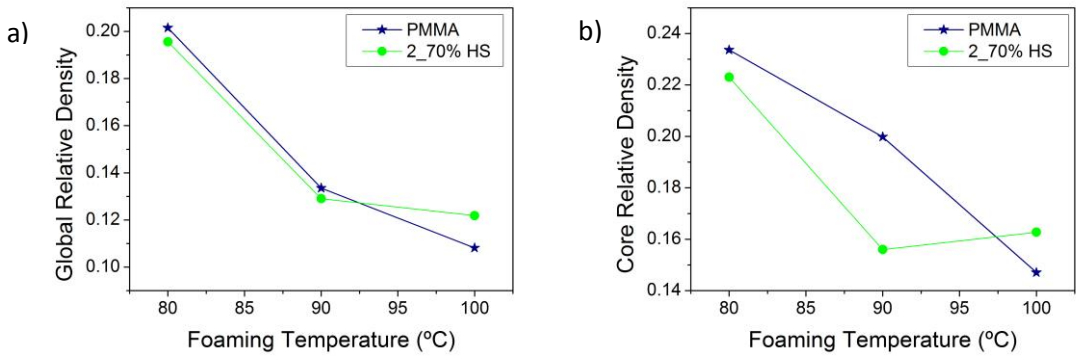

Fig. S1. a) Global and b) core relative densities in function of the foaming temperature.

S2. Analysis of the nanostructuration of the sample 5_80% HS

With the aim to study the nanostructuration, the solid samples were chemical etched with THF during 30 min.

The samples with the highest content of TPU (5 wt%) were the only ones where the SEM reveals the nanostructuration, while in the others nothing could be clearly observed (**Fig. 3** in the main text of this paper). Besides, for the material 5_80% HS the extrusion flow can be observed in the SEM micrographs (**Fig. S2a**). In the centre of the sample, the TPU is well dispersed, as it was observed in **Fig. 3i**. Besides, this region is transparent (**Fig. S2b**). In the regions near the centre, the sample is more opaque (**Fig. S2b**), so TPU should be worse dispersed. Furthermore, this fact explains that the foamed sample did not present a pure gradient structure, rather, it presents a structure as schematically represented in **Fig. S2c**. The green zone is the core, the blue region represents the gradient microcellular structure and the purple areas (which coincide with the position of the extruder screws) are regions with larger cell sizes. Furthermore, **Fig. S2d**, **Fig. S2e** and **Fig. S2f** shows representative SEM images of the cellular material 5_80% HS at different magnifications, where the green area represents the nanocellular core, the not market areas are the transition regions (gradient) and the purple area represents the larger cell sizes areas. Therefore, a good dispersion of the nucleants is important because the nanostructuration control the cellular structure and probably other extrusions conditions are needed for this particular material to obtain a more homogeneous distribution of the dispersed phase.

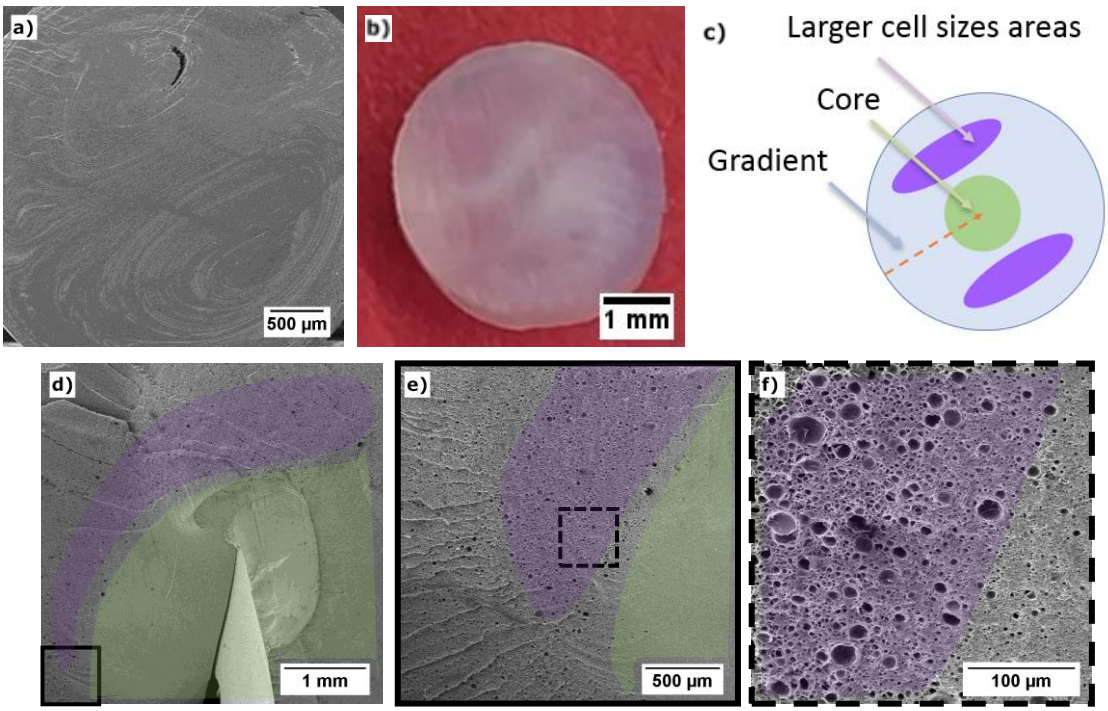

Fig. S2. Material 5_80% HS: a) etched surface in the transversal direction (perpendicular to the extrusion direction), b) solid sample photograph, c) representative cellular structure, e), f) and g) representative SEM images of the cellular material 5_80% HS at different magnifications (green area: nanocellular core, not market areas: transition regions and purple area: larger cell sizes areas).

S3. Analysis of the gradient in the longitudinal direction of the sample 2_70% HS

To analyse the gradient in the longitudinal direction (i.e., the extrusion direction), SEM images have been taken along the sample length (in the direction of the extrusion).

In **Fig. S3a**, SEM images have been taken in a fracture surface in a transversal direction to the extrusion along the sample radius (as seen in **Fig. S4a**), whereas **Fig. S3b** shows images taken by fracturing in the extrusion direction along the sample length centred in the sample centre (**Fig. S4b**). As seen in these images, in both directions the structure in the edge is microcellular, and the cell size decreases towards the sample core, that presents a nanocellular structure. It is observed that the core nanocellular region is reached before in the longitudinal direction (at 2 mm) than in the transversal direction (at 2.75 mm).

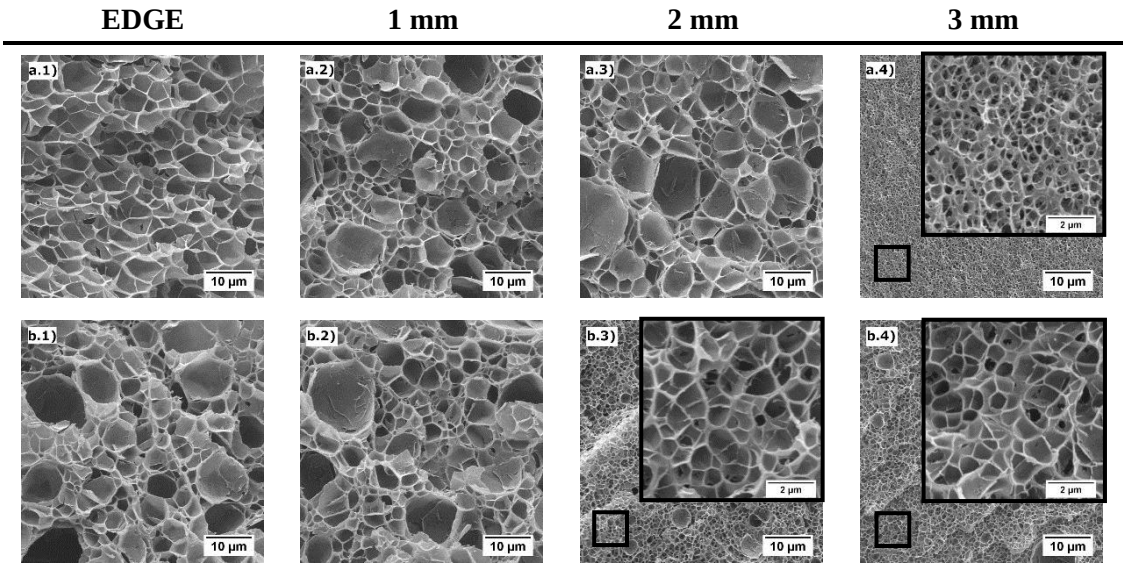

Fig. S3. Representative SEM images of the material 2_70% HS: a) In a transversal direction to the extrusion direction along the sample radius and b) In the extrusion direction along the sample length in the sample centre. Each image is taken at increasing distance from the edge of the sample (a.1 and b.1: EDGE; a.2 and b.2: 1 mm; a.3 and b.3: 2 mm; a.4 and b.4: 3 mm). Images a.4, b.3 and b.4 and have been taken in the core.

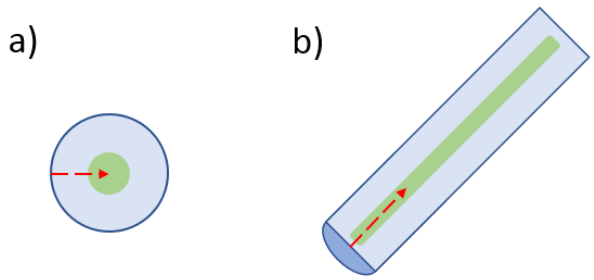

Fig. S4. Schematic representation of: a) fracture in a transversal direction to the extrusion direction, and b) fracture in the extrusion direction. Green area: nanocellular core. Blue area: transition region.

The appearance of a gradient structure on both surfaces indicates a homogeneous dispersion of the TPU phase across the sample radius. Since, otherwise, in the longitudinal direction of the extrusion the gradient would have not been observed. Also, reaching the core previously from the bottom surfaces than from the lateral surface may be due to faster desorption in the lateral area, because the lateral surface area is greater.

S4. Effect of cooling the autoclave before the pressure release

An additional foaming test in which a cooling step is introduced before releasing the pressure has been carried out to study the gradient cellular structure and the bimodality observed in the PMMA/TPU foams. The cooling may allow the samples to achieve more gas (that diffuses from the surface to the centre) near the surface because solubility increases for lower temperatures. Also, by freezing the samples before the pressure release it is harder for the gas to diffuse outwards during depressurization because diffusion constants are reduced when lower temperatures are used

In this experiment, a cooling step before the depressurisation was carried out. To cool the autoclave, ice and liquid nitrogen have been used during 30 min, reaching a temperature of 12 ºC inside the autoclave. When the autoclave was opened, dry ice was formed (temperature of - 66 ºC). The samples included in this test were the pure PMMA sample and the PMMA/TPU blends (the three amounts of HS and the three contents).

S4.1. Analysis of the gradient cellular structure of the sample 2_70%HS

Fig. S5 shows representative SEM images taken at increasing distances from the edge to the centre of the sample along the sample radius for the samples produced at normal conditions (that is, with depressurization at room temperature, **Fig. S5a**) and with the extra cooling step (**Fig. S5b**). The radial distance (r_d), defined as the ratio between the distance from the centre of the sample to the point of observation divided by the simple radius, has been taken for the sake of comparison because samples had different radius. The quantitative analysis of the cellular structure (cell size and cell density) throughout the sample radius is plotted in **Fig. S6**. On the one hand, as already seen in the main text of this paper, the sample produced at normal conditions presents a gradient structure from the edge to the centre (**Fig. S5a**): the cell density increases (**Fig. S6a**) and the cell size decreases (**Fig. S6b**). On the other hand, the cooled sample presents a gradient, but it is more smooth as shown in **Fig. S6** which may be due to the fact that the cooling of the structure reduces the loss of gas. Also, in **Fig. S5b.1** the solid skin can be observed and how exist a gradient of cell size as the distance increase with the opposite behaviour that seen before (the cell density increases and the cell size decreases). However, the concentration of the gas in the surface explains the fact that the cell size in the edge. The cooling may allow the sample to achieve more gas (that diffuses from the surface to the centre) near the surface because

solubility increases for lower temperatures. This reveals the two facts, the loos of gas in the surfaces and the concentration of the gas near the surface. The differences between both tests prove that the gradient structure is caused by the concentration of the gas.

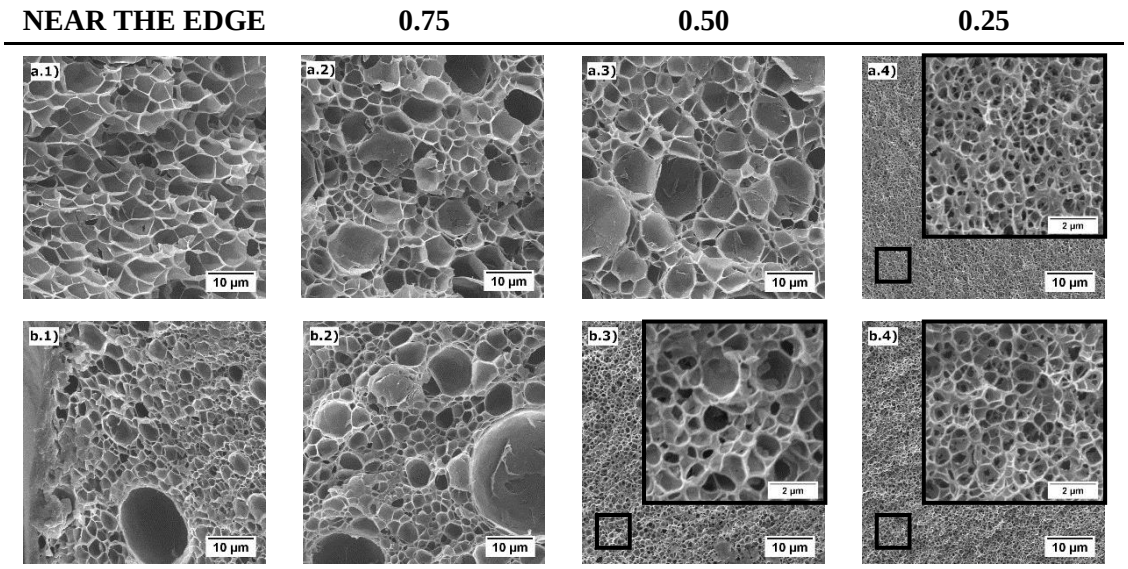

Fig. S5. Representative SEM images of the material 2_70% HS: a) Normal conditions and b) Cooling step before depressurisation. Each image is taken at increasing distance from the edge to the centre of the sample along the sample radius (a.1 and b.1 NEAR THE EDGE (r_d ~ 1); a.2 and b.2: r_d ~ 0.75; a.3 and b.3: r_d ~ 0.50; a.4 and b.4: r_d ~ 0.25). Images a.4, b.3 and b.4 have been taken in the core of the samples.

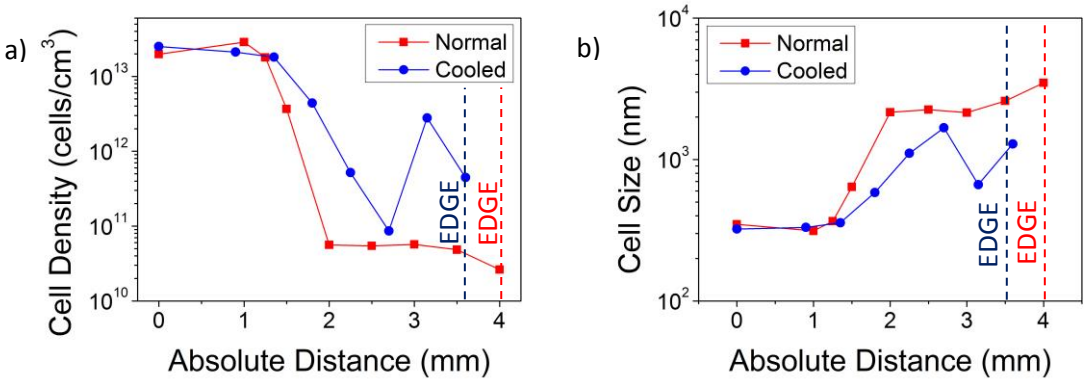

Fig. S6. a) Cell density and b) cell size of the as a function of the radial distance from the centre (0 mm) to the edge of the sample.

In addition, **Table S1** summarizes the analysis of the core nanocellular region of the 2_70% HS material. Firstly, the cooled sample presents higher relative densities than in normal conditions. This may be caused by the cooling, because the sample is cooler, and the structure requires higher foaming times to achieve the same expansion (i.e. the optimum foaming conditions could be different for the experiments in which the cooling step was introduced). Secondly, it is observed, that in the cooled sample the global relative density ($\rho_{r,g}$) and the core relative density ($\rho_{r,c}$) are

almost the same (0.170 versus 0.167 respectively). Regarding the cell size, it is slightly lower (348 nm versus 322 nm in the cooling experiment), but the cell density and the cell nucleation density in both cases are very similar. This is a reasonable result because the nucleation depends on the gas concentration (pressure), and thus, at equal pressure in the core, the same nucleation density should be reached.

Table S1. Cellular characteristics of core region of the sample 2_70% HS.

2_70% HS	$\rho_{r,g}$	$\rho_{r,c}$	ϕ (nm)	SD/ ϕ	N_v (cells/cm^3)	N_0 (nuclei/cm^3)
Normal	0.107	0.156	348	0.52	$2.0 \cdot 10^{13}$	$1.3 \cdot 10^{14}$
Cooled	0.17	0.167	322	0.49	$2.5 \cdot 10^{13}$	$1.5 \cdot 10^{14}$

S4.2. Analysis of the bimodality of several PMMA/TPU samples

Besides the reduction of the thickness of the gradient structure, cooling before releasing the pressure has another effect in the structure of the PMMA/TPU samples. It is observed that the cooling step reduces the bimodality of the nanocellular core as shown representatively in **Fig. S7**. If a poor TPU dispersion was the cause of the bimodality, both cellular structures had to be similar. However, by cooling before releasing the pressure the bimodality is reduced. The cooling reduces the prefoaming, improving the homogeneity of the cellular structure. The fact that bimodality still exists at the lowest contents might be due to the TPU dispersion, the content might be too low to fill homogeneously the sample.

	Normal	Cooled
a) 0.5_60% HS	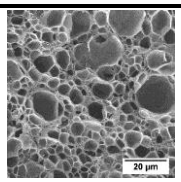	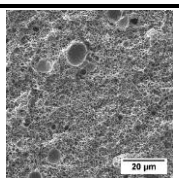
b) 2_60% HS	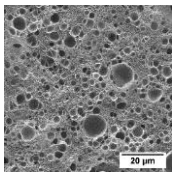	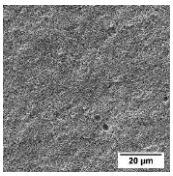
c) 5_60% HS	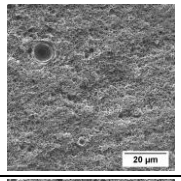	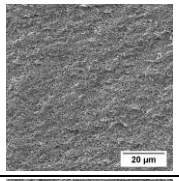
d) 0.5_70% HS	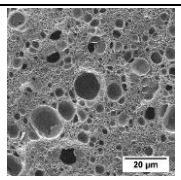	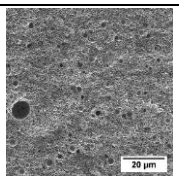
e) 2_70% HS	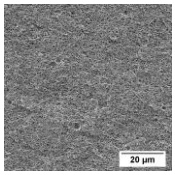	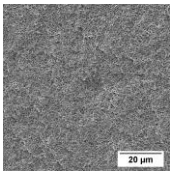
f) 5_70% HS	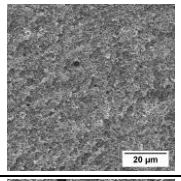	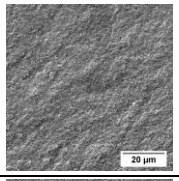
g) 0.5_80% HS	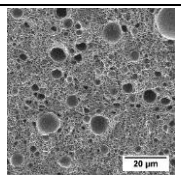	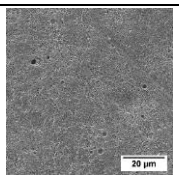
h) 2_80% HS	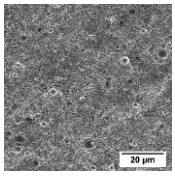	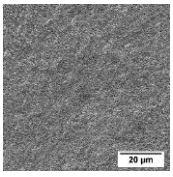
i) 5_80% HS	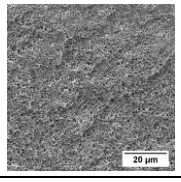	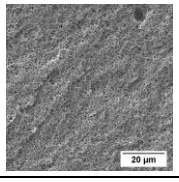

Fig. S7. SEM images of the material: a) 0.5_60% HS, b) 2_60% HS, c) 5_60% HS, d) 0.5_70% HS, e) 2_70% HS, f) 5_70% HS, g) 0.5_80% HS, h) 2_80% HS and i) 5_80% HS. Normal conditions (Left) and cooling step before depressurization (Right).

Fig. S8 shows the global and core relative density of the foamed samples in the normal conditions (**Fig. S8a**) and in the cooling conditions (**Fig. S8b**). It is observed that the cooled samples present higher relative densities than in normal conditions because the structure requires higher foaming times to achieve the same expansion. Also, in the cooling conditions as the TPU content increases the core relative density approaches to the global relative density, even reaching lowers values for some of the samples. One possible reason is that the appearance of cells of smaller sizes near the surface increased the global relative density, while increasing the TPU content, the size of these cells decreases. Further experiments are needed to analyse this interesting result.

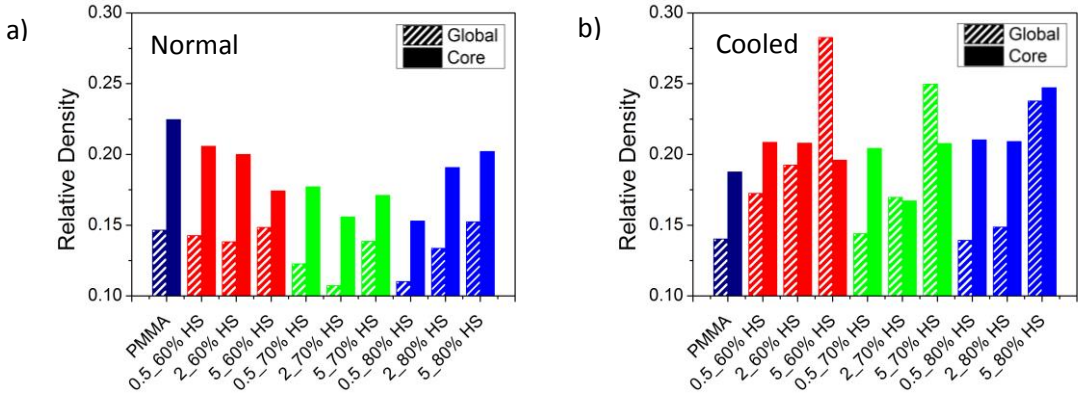

Fig. S8. Global and core relative density of the foamed samples: a) normal conditions and b) cooling step before depressurization.

S5. Cell size distribution of the PMMA/TPU samples

Fig. S9 and **Fig. S10** shows the cell size distributions of the materials produced at 15 MPa of saturation pressure (normal conditions) and foamed at 90 ºC for 1 minute. The nanocellular region is in **Fig. S9** while the microcellular region is in **Fig. S10**.This information completes the data of **Table 5** (in the main text) and supports the discussion about the effect of the TPU content and of the amount of hard segment (HS) in the TPU in the cell size.

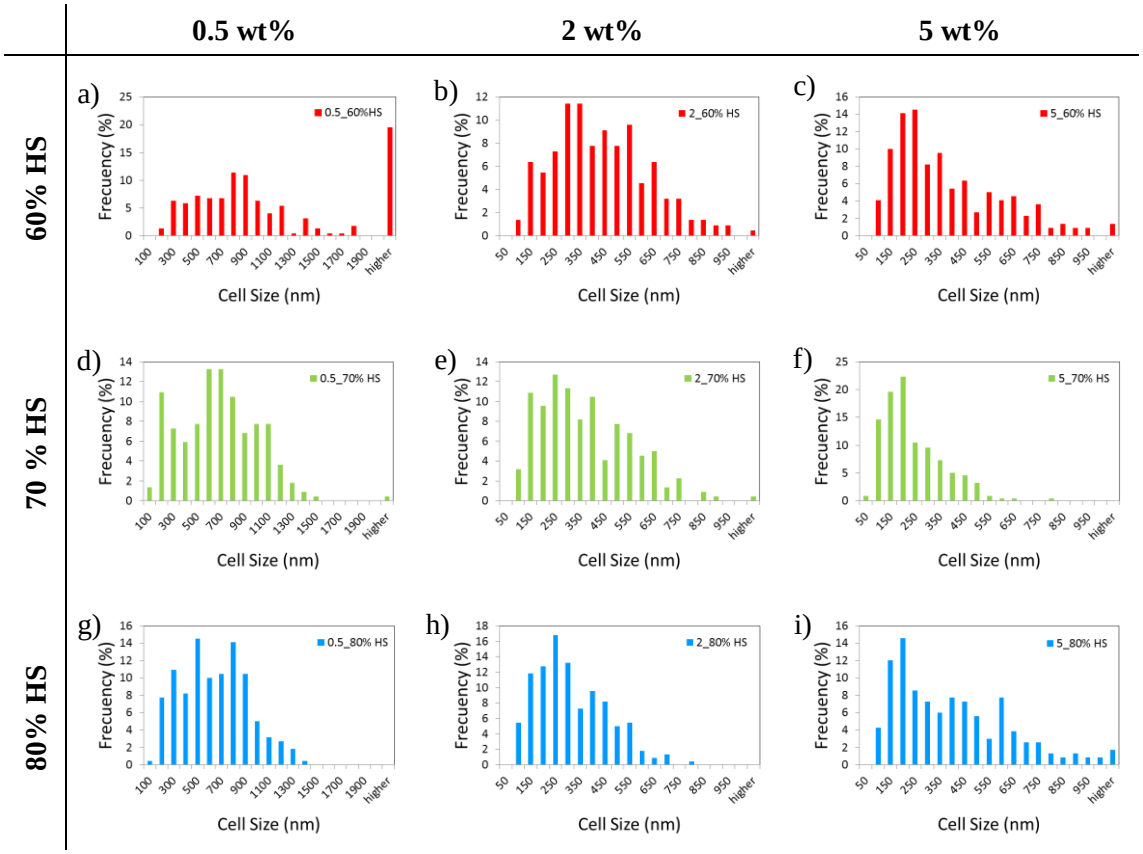

Fig. S9. Core cell size distribution of the nanocellular region of the PMMA/TPU samples produced at normal conditions: a) 0.5_60% HS, b) 2_60% HS, c) 5_60% HS, d) 0.5_70% HS, e) 2_70% HS, f) 5_70% HS, g) 0.5_80% HS, h) 2_80% HS and i) 5_80% HS.

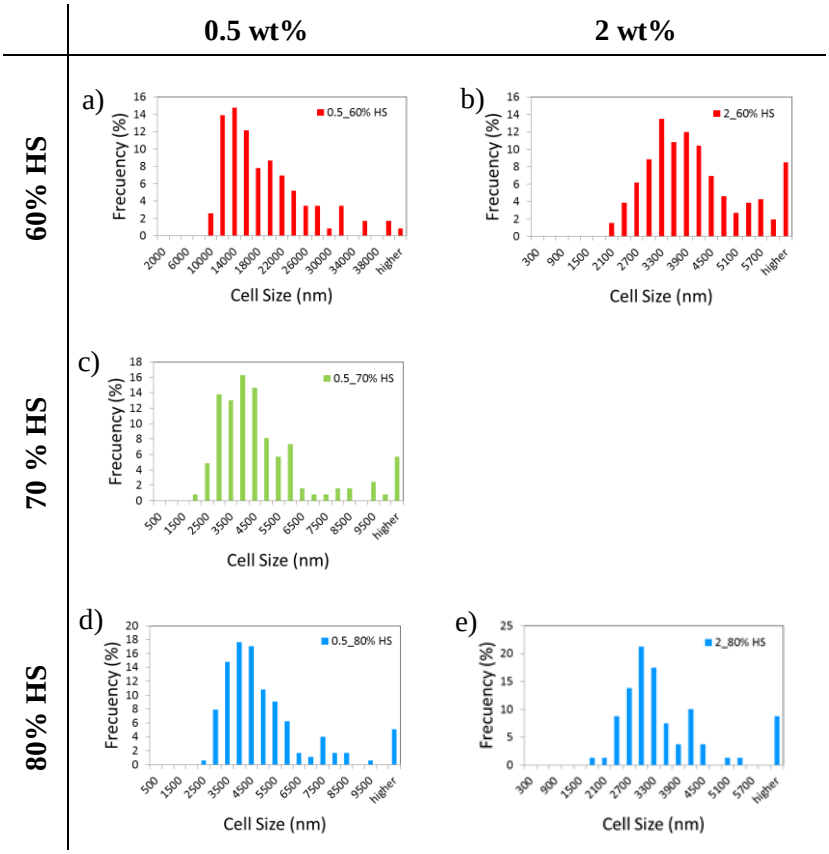

Fig. S10. Core cell size distribution of the microcellular region of the PMMA/TPU samples produced at normal conditions: a) 0.5_60% HS, b) 2_60% HS, c) 0.5_70% HS, d) 0.5_80% HS, e) 2_80% HS.